



**UNIVERSITY OF LEEDS**

This is a repository copy of *Numerical Investigation of Cold-Formed Stainless Steel Lipped Channels with Longitudinal Stiffeners Subjected to Shear*.

White Rose Research Online URL for this paper:  
<https://eprints.whiterose.ac.uk/164430/>

Version: Accepted Version

---

**Article:**

Dissanayake, DMMP, Poologanathan, K, Gunalan, S et al. (3 more authors) (2021)  
Numerical Investigation of Cold-Formed Stainless Steel Lipped Channels with Longitudinal Stiffeners Subjected to Shear. *Thin-Walled Structures*, 158. 107179. ISSN 0263-8231

<https://doi.org/10.1016/j.tws.2020.107179>

---

© 2020, Elsevier. This manuscript version is made available under the CC-BY-NC-ND 4.0 license <http://creativecommons.org/licenses/by-nc-nd/4.0/>.

**Reuse**

This article is distributed under the terms of the Creative Commons Attribution-NonCommercial-NoDerivs (CC BY-NC-ND) licence. This licence only allows you to download this work and share it with others as long as you credit the authors, but you can't change the article in any way or use it commercially. More information and the full terms of the licence here: <https://creativecommons.org/licenses/>

**Takedown**

If you consider content in White Rose Research Online to be in breach of UK law, please notify us by emailing [eprints@whiterose.ac.uk](mailto:eprints@whiterose.ac.uk) including the URL of the record and the reason for the withdrawal request.



[eprints@whiterose.ac.uk](mailto:eprints@whiterose.ac.uk)  
<https://eprints.whiterose.ac.uk/>

1 **Numerical Investigation of Cold-Formed Stainless Steel Lipped**  
2 **Channels with Longitudinal Stiffeners Subjected to Shear**

3  
4 **D. M. M. P. Dissanayake**

5 Faculty of Engineering and Environment, University of Northumbria,  
6 Newcastle, UK.

7 **K. Poologanathan**

8 Faculty of Engineering and Environment, University of Northumbria,  
9 Newcastle, UK.

10 **S. Gunalan**

11 School of Engineering and Built Environment, Griffith University,  
12 Gold Coast, Australia.

13 **K. D. Tsavdaridis**

14 School of Civil Engineering, Faculty of Engineering and Physical Sciences, University of  
15 Leeds, UK.

16 **K. S. Wanniarachchi**

17 Faculty of Engineering, University of Ruhuna, Sri Lanka.

18 **B. Nagaratnam**

19 Faculty of Engineering and Environment, University of Northumbria,  
20 Newcastle, UK.

21  
22 **Abstract**

23 The shear response of the cold-formed stainless steel lipped channel sections with longitudinal  
24 stiffeners has not been investigated adequately in the past. Therefore, this paper presents the  
25 details of numerical investigations conducted to study the shear behaviour of longitudinally  
26 stiffened cold-formed stainless steel lipped channel sections. Following a validation study of  
27 the finite element models of lipped channel sections, the effect of return lips and web stiffeners  
28 on the shear response of lipped channel sections was examined through comprehensive  
29 numerical parametric studies. In addition, numerical investigations were conducted to study  
30 the elastic shear buckling response of the sections and the shear buckling coefficients were  
31 back-calculated. It was found that the longitudinal web stiffeners enhance the shear buckling  
32 resistance of lipped channel sections considerably with increased stiffener depth. However, the

33 shear capacity increment is not significant compared to plain lipped channel sections. The  
34 presence of the web stiffeners is found to be not preventing the out-of-plane buckling of the  
35 sections. The evaluation of Eurocode 3 and the direct strength method shear provisions for  
36 stainless steel channel sections with longitudinal stiffeners illustrated inaccurate capacity  
37 predictions. Therefore, modifications were proposed and comparisons reveal that the proposed  
38 provisions enhance the shear resistance predictions with good accuracy over the codified  
39 provisions.

40 *Keywords: Cold-formed stainless steel, Channel sections, Longitudinal stiffeners, Shear and*  
41 *shear buckling, Eurocode 3, Direct strength method*

## 42 **1 Introduction**

43 Cold-formed sections are commonly used in the construction industry and can be found in a  
44 wider range of applications as structural components such as roof purlins, wall studs and floor  
45 joists. This is mainly because the cold-forming manufacturing techniques such as roll forming  
46 and press braking have made it possible to produce cold-formed sections of high strength-to-  
47 weight ratio. In addition to commonly available cold-formed sections such as C-sections, Z-  
48 sections and hollow sections, complex cross-sectional geometries feature longitudinal  
49 stiffeners to enhance their structural performance. Over the years, many research studies have  
50 been conducted to investigate the structural behaviour of cold-formed steel stiffened sections.  
51 Pham et al. [1] conducted experimental studies on cold-formed steel channel sections with  
52 trapezoidal and rectangular web stiffeners subjected primarily to shear action. Pham and  
53 Hancock [2] tested plain and SupaCee® channel sections for shear, and combined bending and  
54 shear actions. Wang and Young [3] investigated the bending behaviour of cold-formed steel  
55 channel sections with stiffened webs using experiments. Furthermore, Pham et al. [4]  
56 conducted numerical studies on the shear behaviour of cold-formed steel channel sections with  
57 rectangular and triangular web stiffeners. However, less attention has been given on the cold-  
58 formed stainless steel stiffened sections in the past. Therefore, this paper aims to investigate  
59 the shear response of cold-formed stainless steel channel sections with longitudinal stiffeners  
60 using numerical studies.

61 For the design of stainless steel sections, European standards for stainless steel, EN1993-1-4  
62 [5] is available and should be referred with European standards for plated structural elements,  
63 EN1993-1-5 [6]. In the current version of EN1993-1-5 [6], Höglund's [7] rotated stress field  
64 theory is adopted to calculate the shear buckling resistance of sections with both stiffened and

65 unstiffened webs and takes into account the flange contribution to the shear resistance.  
66 However, European standards neglect the beneficial effect of element interaction in the  
67 calculation of section resistance [8]. Alternatively, the direct strength method (DSM) and the  
68 continuous strength method (CSM) have recently been introduced for the design of steel  
69 sections. Both these design approaches deal with the full cross-section buckling, therefore  
70 taking into consideration the element interaction to the section resistance. When calculating the  
71 full cross-section buckling resistance, numerical techniques such as finite strip method (FSM)  
72 and finite element method (FEM) may be associated. The FSM is adopted in software such as  
73 CUFSM [9] and THIN-WALL-2 [10] while there are many commercially available software  
74 packages for FEM. The DSM of design for shear is recently introduced in Australian/New  
75 Zealand standards, AS/NZS 4600 [11] and American specifications, AISI S100 [12] for cold-  
76 formed steel design.

77 In this paper, the details of numerical simulations conducted to investigate the shear behaviour  
78 and the elastic shear buckling behaviour of cold-formed stainless steel channel sections with  
79 longitudinal stiffeners is presented. Based on the numerical results, a set of equations for both  
80 EN1993-1-4 [5] and the DSM was proposed to predict the shear resistance of cold-formed  
81 stainless steel stiffened channel sections.

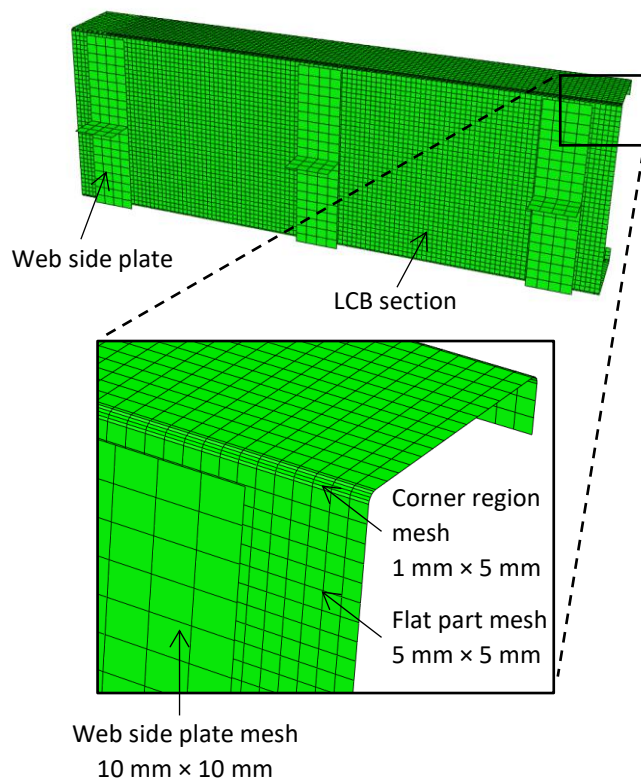
## 82 **2 Finite element (FE) modelling of shear behaviour**

83 The shear behaviour of cold-formed stainless steel lipped channel beams (LCBs) were first  
84 simulated using commercially available FE software package ABAQUS CAE 2017 and the  
85 details of numerical modelling are given in this section. The developed FE models are based  
86 on the three-point loading tests of cold-formed stainless steel LCBs found in Dissanayake et  
87 al. [13]. FE models were developed for eight tests of LCBs with an aspect ratio (shear span ( $a$ )  
88 to clear web depth ( $d_1$ ) ratio) of 1.0. Keerthan and Mahendran [14] showed that when shorter  
89 spans (with  $a/d_1=1.0$ ) are employed in the shear tests, the generated bending moments are of  
90 lower magnitudes, thus no bending-shear interaction is taken place within the sections.  
91 Therefore, this aspect ratio ensures that the shear stresses generated within the sections are  
92 independent of bending stresses. In the experiments, the back-to-back beam arrangement has  
93 been employed to eliminate torsional effects, however, single LCBs were modelled together  
94 with three web side plates in the numerical modelling considering the symmetry of the test  
95 setup. More details on the three-point loading tests and the back-to-back beam setups can be

96 found in [14] for cold-formed steel LCBs and in [15]–[17] for cold-formed steel LiteSteel  
97 beams.

## 98 2.1 Element type and FE mesh

99 Four node shell element type with reduced integration (S4R) was chosen from Abaqus element  
100 library to model sections. This S4R shell element type has six degrees of freedom (DOFs) at  
101 each of its node. The element is ideal for large strain analyses since it accounts for finite  
102 membrane strains and large rotations [18]. A number of studies have previously proven the  
103 successful employment of this element type to simulate the non-linear behaviour of thin  
104 sections [19]–[23]. Mesh sensitivity analyses were conducted and convergence was identified  
105 which provides reasonably accurate results. The sensitivity analyses suggested a 5 mm × 5 mm  
106 mesh for flat parts of the sections. A relatively finer mesh of 1 mm × 5 mm was employed for  
107 corner regions to model the corner curvature. A coarser mesh of 10 mm × 10 mm was assigned  
108 to the web side plates as the attention was given to the steel sections. Fig. 1 illustrates the  
109 assembly of different parts and FE mesh employed in the analyses.



110

111 Fig. 1 Assembly of parts and FE mesh used in the modelling

## 112 2.2 Material modelling of stainless steel

113 Stainless steel exhibits a non-linear stress-strain behaviour with gradual yielding and shows  
114 different levels of strain hardening under higher strain levels in each stainless steel grade. To  
115 represent this non-linear material behaviour, two-stage Ramberg-Osgood material model has  
116 been widely used and a number of modifications have been proposed to the original version of  
117 this model. A recent study by Arrayago et al. [24] proposed modifications to the codified  
118 version of the two-stage Ramberg-Osgood model provided in EN1993-1-4 [5] considering a  
119 large number of stainless steel material data. The two-stage Ramberg-Osgood material model  
120 with Arrayago et al.'s [24] proposals was utilised to represent the stress-strain behaviour of  
121 stainless steel in numerical parametric studies conducted in Section 4 of this study. It is required  
122 to input stress-strain data of a non-linear material in terms of true stress ( $\sigma_{\text{true}}$ ) and log plastic  
123 strain ( $\epsilon_{\text{ln}}^{\text{pl}}$ ) into Abaqus. Therefore, Eqs. (1) and (2) were used to calculate true stress ( $\sigma_{\text{true}}$ )  
124 and log plastic strain ( $\epsilon_{\text{ln}}^{\text{pl}}$ ) values of each stainless steel grade, respectively. A sufficient  
125 number of data sets were fed into Abaqus to accurately model the non-linear material  
126 behaviour.

$$127 \quad \sigma_{\text{true}} = \sigma_{\text{nom}}(1 + \epsilon_{\text{nom}}) \quad (1)$$

$$128 \quad \epsilon_{\text{ln}}^{\text{pl}} = \ln(1 + \epsilon_{\text{nom}}) - \frac{\sigma_{\text{true}}}{E} \quad (2)$$

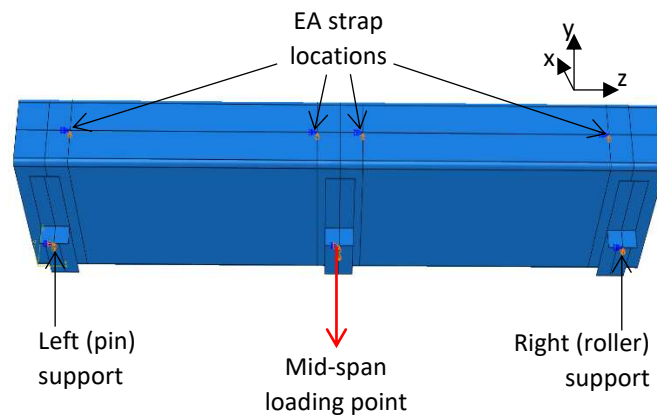
129 where  $\sigma_{\text{nom}}$  and  $\epsilon_{\text{nom}}$  are the engineering stress and strain, respectively and E is Young's  
130 modulus.

131 During the cold-forming process of LCB sections, corner regions undergo plastic deformations.  
132 This leads to a change in material properties, typically associated with enhanced yield and  
133 ultimate stresses. These strength enhancements were explicitly included in the FE modelling  
134 of cold-formed stainless steel LCBs. Cruise and Gardner's [25] predictive model for enhanced  
135 corner 0.2 % proof stress and Ashraf et al.'s [26] proposal for enhanced corner ultimate stress  
136 were employed in Section 4 of this study. More details can be found from Dissanayake et al.  
137 [13].

## 138 2.3 Boundary conditions and loading

139 Boundary conditions were assigned to the FE models such that they accurately simulate the  
140 experimental conditions. Simply supported boundary conditions were maintained at the two

141 beam ends by employing pin and roller support conditions to the end web side plates. This was  
 142 achieved by restraining in-plane translational DOFs in the x-y plane at both these locations and  
 143 restraining translational DOF in the z-direction at the left support. Further, rotational DOF  
 144 about the longitudinal axis (z-axis) of the LCB was restrained at these two supports to eliminate  
 145 any torsional effect. Lateral deflection along the x-axis and the rotation about the z-axis were  
 146 fixed at the respective flange locations to simulate the effect of equal angle straps employed in  
 147 the experiments to avoid distortional buckling of the sections. Mid-span loading was applied  
 148 to the mid web side plate in terms of vertical downward displacement. The interaction between  
 149 LCB web and web side plates due to the bolted connections was modelled by choosing tie  
 150 constraints from Abaqus. Fig. 2 shows the locations of assigned boundary conditions in the FE  
 151 modelling.



152

153 Fig. 2 Locations of the assigned boundary conditions in the FE modelling

#### 154 2.4 Local geometric imperfections

155 The local or global deviations of the section geometry compared to its perfect geometry are  
 156 called geometric imperfections. These imperfections can affect the performance of the  
 157 structure. Therefore, geometric imperfection patterns were identified through numerical  
 158 analyses and included in non-linear FE models using a suitable scaling factor. There were no  
 159 signs of lateral torsional buckling of the sections observed in the experiments conducted by  
 160 Dissanayake et al. [13]. Therefore, only the local geometric imperfections were taken into  
 161 account in this study. Dawson and Walker [27] proposed a model for imperfection magnitude  
 162 ( $\omega_0$ ) and this has been modified by Gardner and Nethercot [28]. This is given in Eq. (3) and  
 163 was employed in this study to calculate the scaling factor.

164  $\omega_0 = 0.023 \left( \frac{\sigma_{0.2}}{\sigma_{cr}} \right) t$  (3)

165 where  $\sigma_{0.2}$  is the 0.2 % proof stress of the material,  $\sigma_{cr}$  is the lowest value of the critical elastic  
166 buckling stress calculated for the constituent plate elements of the section and  $t$  is the thickness.

### 167 2.5 Eigenvalue buckling analysis

168 An Eigenvalue buckling analysis was performed on each FE model to obtain the elastic  
169 buckling mode shapes of the section under the applied boundary conditions and loading  
170 patterns. From the generated buckling modes, critical buckling mode shapes were identified  
171 which are usually corresponding to the lowest Eigenmodes. These elastic buckling modes were  
172 taken as the initial geometric imperfection patterns of the sections and incorporated to perturb  
173 the section geometry in the non-linear analyses. Inputs to extract the relevant elastic buckling  
174 mode shapes with suitable scaling factors were given through command lines as instructed in  
175 user manuals [18].

### 176 2.6 Geometrically and materially non-linear analysis

177 A modified Static, Riks analysis was performed on the developed FE models to study the  
178 collapse mechanism and post-buckling response of the sections with due consideration giving  
179 to geometrically and materially non-linear effects. The effects of initial geometric  
180 imperfections were also added in the non-linear analysis to perturb the mesh. Subsequently,  
181 the ultimate loads of the sections at the failure were obtained from the load-displacement curves  
182 and the structural response of the sections was studied.

## 183 3 Validation of FE models for shear behaviour

184 The results obtained from the FE models of cold-formed stainless steel LCB sections which  
185 subjected to shear were compared with the experimental results of corresponding tests found  
186 from Dissanayake et al. [13]. The details of these comparisons are elaborated in this section.  
187 The measured geometric and material properties were utilised in the FE models developed for  
188 validation. Table 1 compares the experimental and FE ultimate shear capacities ( $V_{Exp.}$  and  $V_{FE}$ ).  
189 The format, section name followed by section depth (D) × section breadth (B) × lip height (L)  
190 × thickness (t) was adopted throughout this paper to designate the sections. From the results, it  
191 can be seen that the mean and the coefficient of variation (COV) of the experimental shear  
192 capacity to the FE shear capacity ratio are 1.02 and 0.073, respectively. Therefore, it can be



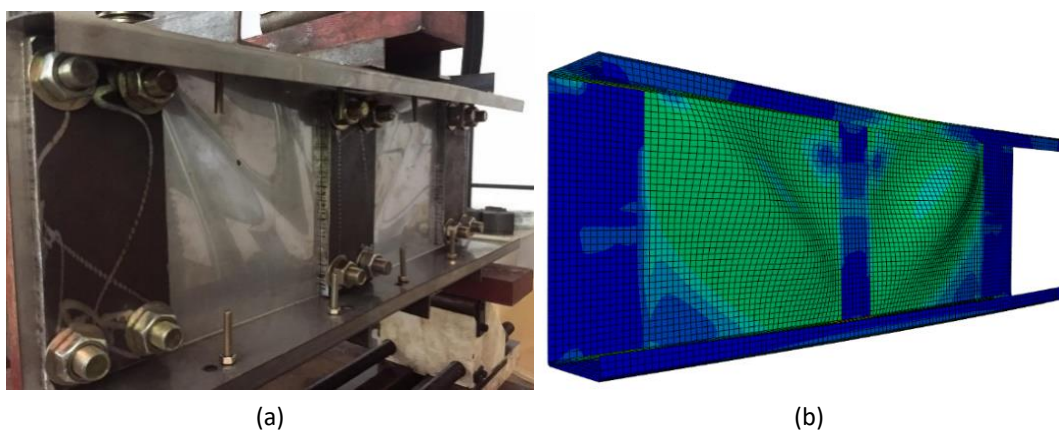
193 concluded that the developed FE models predict the shear capacity of LCB sections with  
194 reasonably good accuracy.

195 Table 1 Experimental [13] and FE shear capacities for cold-formed stainless steel LCBs

LCB section	$V_{Exp.}$ (kN)	$V_{FE}$ (kN)	$V_{Exp.}/V_{FE}$
LCB 100×50×15×1.2	18.49	16.86	1.10
LCB 100×50×15×1.5	24.44	23.90	1.02
LCB 100×50×15×2.0	36.00	32.72	1.10
LCB 150×65×15×1.2	21.60	20.09	1.08
LCB 150×65×15×1.5	26.26	28.40	0.92
LCB 150×65×15×2.0	43.55	42.60	1.02
LCB 200×75×15×1.2	22.98	22.97	1.00
LCB 200×75×15×2.0	47.05	52.11	0.90
Mean			1.02
COV			0.073

196

197 Further, experimental and FE shear failure modes were compared in Fig. 3. From Fig. 3, it is  
198 seen that the FE model is able to capture the diagonal shear failure of both webs in a fairly  
199 similar manner to the experimental failure mode. Therefore, it can be concluded that the shear  
200 behaviour of cold-formed stainless steel LCBs is well captured from these numerical models.



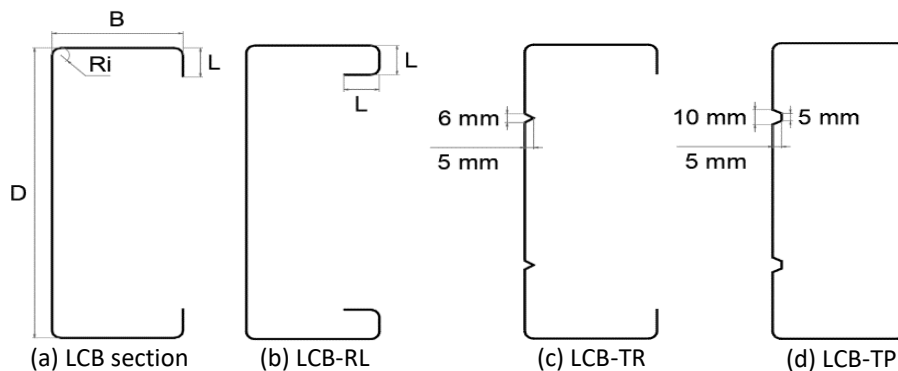
201

202 Fig. 3 (a) Experimental [13] and (b) FE shear failure modes of cold-formed stainless steel LCB 200×75×15×1.2  
203 section

204 **4 Parametric study**

205 4.1 General

206 The validated FE models of cold-formed stainless steel LCBs were then utilised in investigating  
207 the effect of different key parameters on the shear response of cold-formed stainless steel  
208 stiffened sections. Different types of longitudinal stiffeners were introduced to the LCB  
209 sections in the numerical modelling to accomplish this task. The details of cross-sections  
210 investigated herein are given in Fig. 4 alongside the key dimensions of a LCB section. In Fig.  
211 4, the overall depth of the stiffeners is shown. The first section (LCB-RL) to study was a LCB  
212 section with return lips. The considered return lips were equal in length to lip depth. The second  
213 section (LCB-TR) was a LCB section with two triangular web stiffeners placed at one fourth  
214 and three fourths of the web height. Each triangular stiffener was 6 mm in height and 5 mm in  
215 depth. The third section (LCB-TP) was similar to the second one but trapezoidal web stiffeners  
216 were employed instead of triangular stiffeners. Each trapezoidal stiffener had a 10 mm outer  
217 height which reduces to 5 mm at a 5 mm depth.



219 Fig. 4 Cross-section details of LCB section and stiffened sections

220 Table 2 summarises the different parameters considered to study the shear behaviour of  
221 stiffened LCB sections illustrated in Fig. 4. The effect of three different section depths, four  
222 different section thicknesses, and four different stainless steel grades was investigated in the  
223 parametric study to generate a numerical database. 48 FE models were developed for each  
224 section, therefore, generating 144 FE models in total. Then, the gathered numerical results were  
225 utilised in understanding the shear behaviour of stainless steel stiffened sections and to evaluate  
226 the design rules.

227

228

229 Table 2 Summary of the parameters

Section	Depth, D (mm)	Thickness, t (mm)	Stainless steel grade
LCBs with return lips (LCB-RL)	150, 200, 250	1, 1.2, 1.5, 2	Austenitic-1.4301, 1.4311
LCBs with triangular web stiffeners (LCB-TR)			Duplex-1.4362, 1.4462
LCBs with trapezoidal web stiffeners (LCB-TP)			

230

231 4.2 Summary of generated numerical results

232 The ultimate shear resistances of each section for each stainless steel grade obtained from the  
 233 numerical parametric study are given in Tables 3-5. When developing the FE models in the  
 234 parametric study, Young’s modulus and Poisson’s ratio were taken as 200,000 MPa and 0.3,  
 235 respectively according to EN1993-1-4 [5]. All the developed sections have an aspect ratio of  
 236 1.0 to govern the shear failure.

237 Table 3 Parametric study results with EN1993-1-4 [5] and the DSM predictions for LCB-RL sections

Section	Stainless steel grade – 1.4301					Stainless steel grade – 1.4311					Stainless steel grade – 1.4362					Stainless steel grade – 1.4462				
	$V_{FE}$	$V_{FE}/V_{EC3}$	$V_{FE}/V_{EC3, Proposed}$	$V_{FE}/V_{DSM}$	$V_{FE}/V_{DSM, Proposed}$	$V_{FE}$	$V_{FE}/V_{EC3}$	$V_{FE}/V_{EC3, Proposed}$	$V_{FE}/V_{DSM}$	$V_{FE}/V_{DSM, Proposed}$	$V_{FE}$	$V_{FE}/V_{EC3}$	$V_{FE}/V_{EC3, Proposed}$	$V_{FE}/V_{DSM}$	$V_{FE}/V_{DSM, Proposed}$	$V_{FE}$	$V_{FE}/V_{EC3}$	$V_{FE}/V_{EC3, Proposed}$	$V_{FE}/V_{DSM}$	$V_{FE}/V_{DSM, Proposed}$
LCB-RL 150×65×15×1.0	15.39	1.10	1.01	1.06	1.01	18.32	1.12	1.01	1.09	1.02	24.55	1.11	1.00	1.09	1.01	26.3	1.10	0.99	1.10	1.00
LCB-RL 150×65×15×1.2	20.15	1.09	1.00	1.02	1.00	24.34	1.11	1.02	1.06	1.02	33.45	1.12	1.02	1.09	1.03	36.01	1.12	1.01	1.10	1.03
LCB-RL 150×65×15×1.5	27.73	1.08	1.00	0.98	0.97	33.38	1.09	1.00	1.01	0.99	47.18	1.11	1.02	1.06	1.02	51.02	1.12	1.02	1.07	1.02
LCB-RL 150×65×15×2.0	40.82	1.01	0.96	1.04	1.04	49.78	1.07	0.98	1.01	1.01	70.87	1.08	1.00	0.99	0.98	76.89	1.08	1.00	1.00	0.99
LCB-RL 200×75×20×1.0	17.5	1.12	1.01	1.10	1.02	20.58	1.13	1.01	1.12	1.02	27.2	1.12	0.99	1.12	0.99	28.89	1.11	0.99	1.11	0.98
LCB-RL 200×75×20×1.2	23.67	1.13	1.02	1.09	1.03	28.25	1.14	1.03	1.12	1.04	37.11	1.12	1.00	1.11	1.01	39.46	1.11	0.99	1.11	1.00
LCB-RL 200×75×20×1.5	32.06	1.07	0.98	1.02	0.98	38.78	1.10	1.00	1.06	1.01	53.76	1.12	1.01	1.10	1.02	58.08	1.13	1.02	1.11	1.03
LCB-RL 200×75×20×2.0	48.68	1.06	0.98	0.96	0.96	58.52	1.07	0.99	0.99	0.97	82.25	1.09	0.99	1.04	1.00	89.25	1.09	1.00	1.05	1.00
LCB-RL 250×75×20×1.0	19.02	1.13	1.01	1.12	1.01	22.25	1.14	1.01	1.14	1.00	28.87	1.12	0.99	1.12	0.96	30.5	1.11	0.98	1.11	0.94
LCB-RL 250×75×20×1.2	25.18	1.10	0.99	1.09	1.00	30.15	1.13	1.01	1.12	1.02	39.5	1.11	0.99	1.11	0.98	41.85	1.10	0.98	1.10	0.96
LCB-RL 250×75×20×1.5	35.39	1.08	0.98	1.05	0.99	42.33	1.10	0.99	1.08	1.00	58.52	1.13	1.01	1.12	1.02	62.5	1.12	1.00	1.12	1.01
LCB-RL 250×75×20×2.0	53.38	1.04	0.95	0.97	0.95	64.61	1.06	0.97	1.01	0.97	90.35	1.09	0.98	1.06	0.99	97.79	1.09	0.99	1.07	1.00
Mean		1.08	0.99	1.04	1.00		1.10	1.00	1.07	1.01		1.11	1.00	1.09	1.00		1.11	1.00	1.09	1.00
COV		0.033	0.022	0.052	0.029		0.026	0.018	0.050	0.021		0.014	0.012	0.038	0.020		0.012	0.014	0.032	0.025

239 Table 4 Parametric study results with EN1993-1-4 [5] and the DSM predictions for LCB-TR sections

Section	Stainless steel grade – 1.4301					Stainless steel grade – 1.4311					Stainless steel grade – 1.4362					Stainless steel grade – 1.4462				
	$V_{FE}$	$V_{FE}/V_{EC3}$	$V_{FE}/V_{EC3, Proposed}$	$V_{FE}/V_{DSM}$	$V_{FE}/V_{DSM, Proposed}$	$V_{FE}$	$V_{FE}/V_{EC3}$	$V_{FE}/V_{EC3, Proposed}$	$V_{FE}/V_{DSM}$	$V_{FE}/V_{DSM, Proposed}$	$V_{FE}$	$V_{FE}/V_{EC3}$	$V_{FE}/V_{EC3, Proposed}$	$V_{FE}/V_{DSM}$	$V_{FE}/V_{DSM, Proposed}$	$V_{FE}$	$V_{FE}/V_{EC3}$	$V_{FE}/V_{EC3, Proposed}$	$V_{FE}/V_{DSM}$	$V_{FE}/V_{DSM, Proposed}$
LCB-TR 150×65×15×1.0	17.04	1.03	1.04	0.95	1.04	20.29	1.04	1.05	0.97	1.05	27.23	1.01	1.04	0.98	1.03	29.06	1.00	1.03	0.97	1.03
LCB-TR 150×65×15×1.2	21.37	1.02	1.01	0.92	1.00	25.74	1.03	1.02	0.95	1.02	34.47	1.00	1.00	0.95	1.00	36.92	0.99	1.00	0.95	1.00
LCB-TR 150×65×15×1.5	28.26	1.01	0.97	0.95	0.95	34.31	1.03	0.99	0.92	0.98	48.21	1.03	1.01	0.96	1.01	52.16	1.03	1.01	0.97	1.01
LCB-TR 150×65×15×2.0	40.80	0.91	1.01	1.04	1.04	49.70	0.99	1.02	1.01	1.01	70.93	1.03	0.97	0.93	0.97	77.52	1.04	0.98	0.95	0.98
LCB-TR 200×75×20×1.0	18.26	0.99	1.00	0.95	1.00	21.28	0.98	1.00	0.95	1.00	27.67	0.94	0.97	0.93	0.96	29.81	0.95	0.98	0.94	0.97
LCB-TR 200×75×20×1.2	24.67	1.04	1.03	0.98	1.03	28.91	1.03	1.03	0.99	1.03	38.43	1.01	1.02	0.99	1.02	41.30	1.01	1.02	0.99	1.02
LCB-TR 200×75×20×1.5	33.35	1.03	1.00	0.96	1.00	40.49	1.05	1.03	0.99	1.03	55.34	1.05	1.03	1.02	1.05	59.31	1.05	1.03	1.02	1.05
LCB-TR 200×75×20×2.0	49.37	1.03	0.97	0.93	0.96	59.73	1.04	0.99	0.95	0.99	84.40	1.06	1.02	1.00	1.03	91.60	1.07	1.02	1.01	1.04
LCB-TR 250×75×20×1.0	19.50	0.98	1.00	0.97	1.00	22.69	0.98	1.00	0.97	1.00	29.76	0.96	1.00	0.96	0.98	31.51	0.95	0.99	0.96	0.97
LCB-TR 250×75×20×1.2	26.24	1.02	1.02	0.99	1.02	30.95	1.02	1.03	1.01	1.03	41.04	1.01	1.03	1.01	1.03	43.67	1.00	1.02	1.00	1.02
LCB-TR 250×75×20×1.5	36.86	1.04	1.01	0.99	1.02	44.02	1.05	1.03	1.02	1.04	59.91	1.06	1.05	1.04	1.06	64.32	1.06	1.05	1.05	1.06
LCB-TR 250×75×20×2.0	54.44	1.02	0.96	0.95	0.97	65.91	1.04	0.99	0.98	1.00	91.46	1.05	1.01	1.02	1.03	99.81	1.06	1.03	1.04	1.05
Mean		1.01	1.00	0.97	1.00		1.02	1.01	0.98	1.01		1.02	1.01	0.98	1.01		1.02	1.01	0.99	1.02
COV		0.035	0.025	0.033	0.029		0.026	0.021	0.029	0.023		0.037	0.023	0.037	0.030		0.040	0.022	0.038	0.031

241 Table 5 Parametric study results with EN1993-1-4 [5] and the DSM predictions for LCB-TP sections

Section	Stainless steel grade – 1.4301					Stainless steel grade – 1.4311					Stainless steel grade – 1.4362					Stainless steel grade – 1.4462				
	$V_{FE}$	$V_{FE}/V_{EC3}$	$V_{FE}/V_{EC3, Proposed}$	$V_{FE}/V_{DSM}$	$V_{FE}/V_{DSM, Proposed}$	$V_{FE}$	$V_{FE}/V_{EC3}$	$V_{FE}/V_{EC3, Proposed}$	$V_{FE}/V_{DSM}$	$V_{FE}/V_{DSM, Proposed}$	$V_{FE}$	$V_{FE}/V_{EC3}$	$V_{FE}/V_{EC3, Proposed}$	$V_{FE}/V_{DSM}$	$V_{FE}/V_{DSM, Proposed}$	$V_{FE}$	$V_{FE}/V_{EC3}$	$V_{FE}/V_{EC3, Proposed}$	$V_{FE}/V_{DSM}$	$V_{FE}/V_{DSM, Proposed}$
LCB-TP 150×65×15×1.0	17.25	0.97	1.01	0.87	1.02	20.97	0.99	1.04	0.90	1.04	28.80	0.98	1.04	0.92	1.03	30.52	0.96	1.03	0.91	1.01
LCB-TP 150×65×15×1.2	21.75	0.97	0.99	0.91	0.99	26.43	0.98	1.01	0.88	1.01	37.52	1.00	1.04	0.93	1.03	40.49	0.99	1.04	0.93	1.03
LCB-TP 150×65×15×1.5	29.21	0.92	0.98	0.99	0.99	35.56	0.99	0.98	0.95	0.99	50.83	1.01	1.02	0.92	1.01	55.39	1.02	1.03	0.93	1.02
LCB-TP 150×65×15×2.0	40.98	0.91	0.97	1.05	1.05	49.92	0.89	0.98	1.01	1.01	71.48	0.99	0.96	0.93	0.95	77.95	0.99	0.96	0.91	0.95
LCB-TP 200×75×20×1.0	19.90	0.99	1.04	0.93	1.03	22.84	0.96	1.01	0.92	1.00	29.91	0.92	0.99	0.90	0.97	31.59	0.91	0.97	0.89	0.95
LCB-TP 200×75×20×1.2	25.70	1.00	1.02	0.93	1.02	30.10	0.98	1.02	0.93	1.01	38.99	0.93	0.97	0.90	0.96	41.68	0.92	0.97	0.90	0.96
LCB-TP 200×75×20×1.5	34.79	1.01	1.00	0.92	1.00	41.76	1.01	1.02	0.94	1.01	56.05	0.99	1.00	0.94	1.00	59.93	0.98	0.99	0.94	0.99
LCB-TP 200×75×20×2.0	50.17	1.01	0.96	0.95	0.95	61.19	1.02	0.99	0.92	0.98	85.31	1.02	1.00	0.95	1.00	92.57	1.03	1.00	0.96	1.01
LCB-TP 250×75×20×1.0	19.95	0.92	0.97	0.89	0.95	22.57	0.89	0.94	0.87	0.92	29.32	0.86	0.92	0.85	0.89	31.25	0.85	0.92	0.85	0.89
LCB-TP 250×75×20×1.2	27.71	0.99	1.02	0.95	1.01	31.95	0.97	1.00	0.94	0.99	41.54	0.93	0.98	0.92	0.96	44.28	0.93	0.97	0.92	0.96
LCB-TP 250×75×20×1.5	37.57	0.99	0.99	0.93	0.99	44.32	0.99	0.99	0.95	0.99	59.87	0.98	1.00	0.96	1.00	63.16	0.96	0.98	0.94	0.98
LCB-TP 250×75×20×2.0	55.68	1.00	0.96	0.92	0.96	66.93	1.01	0.98	0.94	0.98	94.00	1.03	1.01	0.99	1.02	101.60	1.03	1.02	1.00	1.03
Mean		0.97	0.99	0.94	0.99		0.97	1.00	0.93	0.99		0.97	0.99	0.93	0.98		0.96	0.99	0.92	0.98
COV		0.037	0.026	0.048	0.030		0.045	0.026	0.039	0.028		0.052	0.034	0.036	0.041		0.056	0.035	0.040	0.043

## 243 **5 FE modelling of elastic shear buckling behaviour**

### 244 5.1 General

245 In general, the design of steel sections for shear is associated with the calculation of elastic  
246 shear buckling stresses. European standards for the design of stainless steel, EN1993-1-4 [5]  
247 adopt the equations given in European standards for plated steel, EN1993-1-5 [6] for the  
248 calculation of shear buckling coefficients of constituent plate elements of a section. In addition,  
249 European standards for cold-formed steel, EN1993-1-3 [29] employs separate provisions for  
250 the shear buckling coefficient calculation which usually deals with cumbersome calculations,  
251 in particular when intermediate stiffeners are present.

252 Alternatively, the DSM considers the buckling of whole cross-sections in the shear buckling  
253 coefficient calculation. Therefore, the aid of numerical tools is sought when determining the  
254 solutions for the shear buckling of thin-walled sections in the DSM. The use of FSM and FEM  
255 is more common in achieving this. The shear buckling of cold-formed channel sections with  
256 plain webs has been investigated by Pham and Hancock [30] while that for sections with both  
257 plain and longitudinally stiffened webs has been studied by Pham et al. [4] and Hancock and  
258 Pham [31] using FSM. Further, Keerthan and Mahendran [32], [33] incorporated FEM in  
259 determining the shear buckling characteristics of cold-formed sections including LCBs. In this  
260 study, FEM was utilised to investigate the elastic shear buckling response of the considered  
261 cold-formed LCB cross-sections with stiffeners.

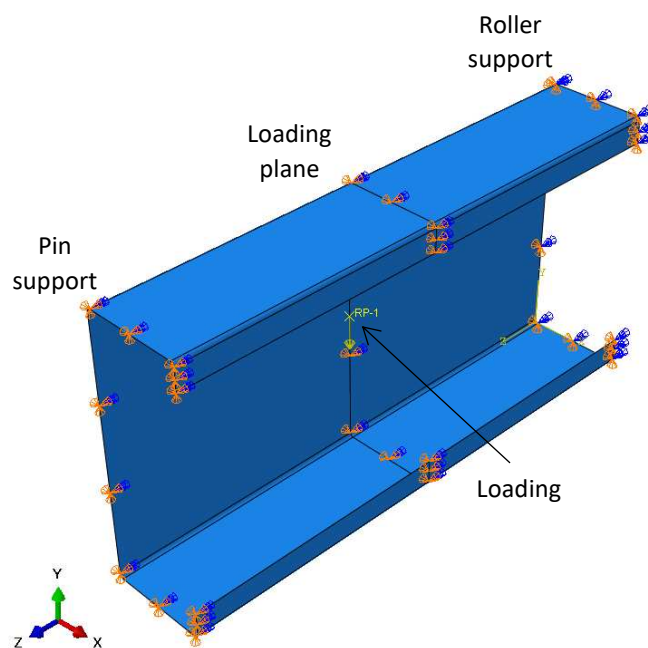
### 262 5.2 FE model development

263 The details of FE modelling carried out to investigate the elastic shear buckling behaviour of  
264 cold-formed stainless steel channel sections with stiffeners are briefed in this section. Abaqus  
265 software was utilised for this purpose.

266 In the FE modelling conducted to study the shear buckling behaviour, the channel sections  
267 were simulated without any transverse stiffeners or flange restraints as opposed to the shear FE  
268 models described in Section 2. A mid-span load was applied to the simply supported sections  
269 with an aspect ratio of 1.0 to simulate the shear buckling behaviour. Four node quadrilateral  
270 S4R shell elements with six DOFs at each node were employed to model the shear buckling  
271 behaviour of thin steel sections. As described in Section 2.1, a 5 mm × 5 mm mesh was assigned  
272 to the flat parts and a relatively finer mesh of 1 mm × 5 mm was employed to the corner regions

273 of the sections. Modified two-stage Ramberg-Osgood material model [24] was adopted here as  
274 well to represent stainless steel behaviour under shear buckling. Young's modulus was taken  
275 as 200,000 MPa and a value of 0.3 was used for Poisson's ratio.

276 Boundary conditions were chosen appropriately. Pin and roller support conditions were  
277 maintained at the two section ends to simulate the simply supported conditions. For this, in-  
278 plane translations were restrained in the cross-sectional plane (x-y plane) at both ends and out-  
279 of-plane translations (in the z-direction) of the cross-sectional plane was restrained at the left  
280 end. Further, rotation about the longitudinal axis (z-axis) of the section was fixed at both ends  
281 to suppress torsional effects. At the mid-span of the section, translations in the x-z plane and  
282 rotation about the z-axis were restrained to provide roller support conditions to the loading  
283 plane. All these restraints were assigned to the entire cross-sections including webs, flanges  
284 and lips to take into account the effect of the shear flow of the full cross-section to the shear  
285 buckling. To generate shear buckling behaviour in the sections, a 1 kN force was applied to the  
286 section web at the mid-span. Fig. 5 illustrates the assigned boundary conditions in the FE  
287 models to study the shear buckling behaviour of LCB sections.



288

289 Fig. 5 Boundary conditions assigned to LCBs in the shear buckling analysis

290 Then, an Eigenvalue buckling analysis was performed on each section. From the results,  
291 Eigenmodes and corresponding Eigenvalues were extracted. The Eigenmodes represent the  
292 elastic shear buckling behaviour of the section and corresponding Eigenvalues provide the



293 shear buckling force of the respective mode. The critical elastic shear buckling modes and  
294 corresponding shear buckling forces were identified for each varying cross-section considered  
295 in the study. Usually, the lowest values are taken as critical.

### 296 5.3 Calculation of shear buckling coefficients

297 Timoshenko and Gere [34] investigated the shear buckling behaviour of flat rectangular plates  
298 and derived an equation to calculate the elastic shear buckling stress ( $\tau_{cr}$ ) of a thin plate. When  
299 the plate is simply supported at its four edges and is subjected to shear stresses, out-of-plane  
300 buckling stress is given by Eq. (4) according to Timoshenko and Gere [34].

$$301 \tau_{cr} = \frac{k_v \pi^2 E}{12(1-\nu^2)} \left( \frac{t}{d_1} \right)^2 \quad (4)$$

302 where E is Young's modulus,  $\nu$  is Poisson's ratio, t is plate thickness and  $d_1$  is plate height.  $k_v$   
303 is the shear buckling coefficient of the plate which depends on the aspect ratio of the plate and  
304 the edge conditions of the plate. The shear buckling coefficient of a simply supported plate  
305 varies from 5.34 for a very lengthy plate to 9.34 for a square plate.

306 Eq. (4) can be applied to cross-section webs if the corresponding shear buckling coefficient of  
307 the section is known. Unlike the simply supported plates, the presence of flanges at the top and  
308 bottom edges enhances the shear buckling resistance of the cross-section webs. The  
309 intermediate web stiffeners further increase the buckling resistance. The use of numerical tools  
310 allows taking into account the behaviour of full cross-sections including the flanges to the shear  
311 buckling of section webs. The effect of intermediate web stiffeners can also be treated in the  
312 analysis. The shear buckling force ( $V_{cr}$ ) of a section web can be related to the shear buckling  
313 stress given in Eq. (4) using the cross-sectional area of the web. Therefore, the shear buckling  
314 coefficient can be back-calculated from Eq. (4) if the shear buckling force of the section web  
315 is known from the numerical analysis.

316 Keerthan and Mahendran [30] proposed an equation for the calculation of the shear buckling  
317 coefficients of cold-formed sections using FE results and is expressed by Eq. (5).

$$318 k_v = k_{ss} + n(k_{sf} - k_{ss}) \quad (5)$$

319 where  $k_{ss}$  and  $k_{sf}$  are the shear buckling coefficients of the web plates with simple-simple and  
320 simple-fixed end conditions, respectively. The coefficient 'n' accounts for the level of fixity at  
321 the web to flange junction which depends on the geometry of the cold-formed section. A value

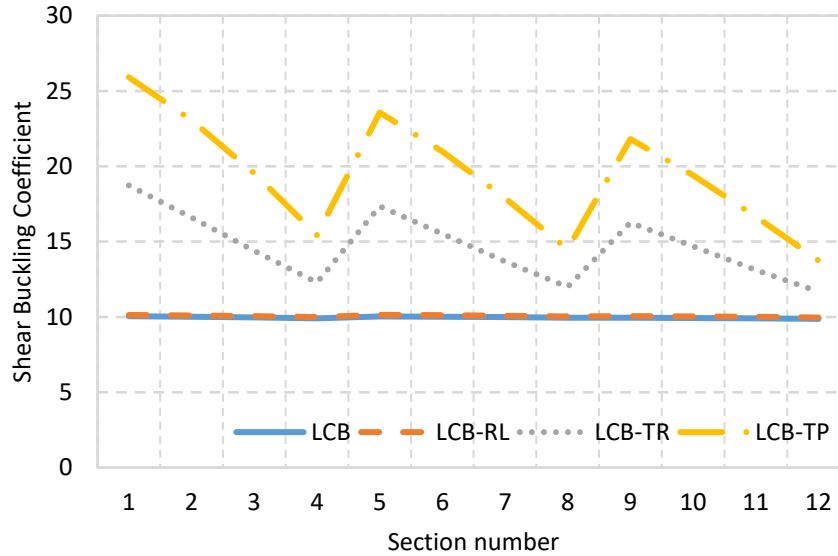
322 of  $n=0.23$  was suggested for LCBs by Keerthan and Mahendran [29]. Therefore, the shear  
323 buckling coefficient of LCB sections with an aspect ratio of 1.0 is equal to a value of 10.09  
324 according to Eq (5).

325 From the elastic shear buckling analysis conducted in Section 5.2, Eigenvalues were extracted  
326 for each section considered and these were incorporated in back-calculating the shear buckling  
327 coefficient of each section. First, the calculated shear buckling coefficients of LCBs were  
328 compared with Eq. (5) to confirm the accuracy of the numerical model to predict the shear  
329 buckling force of the section. Table 6 summarises all the numerical results generated in the  
330 shear buckling analysis, the back-calculated shear buckling coefficients for each section and  
331 the comparison of shear buckling coefficients of each section with the shear buckling  
332 coefficient of LCB sections calculated from Eq. (5). From the comparison, it can be seen that  
333 the ratio between the back-calculated coefficient and the coefficient derived from Eq. (5) for  
334 LCBs has a mean and a COV of 0.99 and 0.006, respectively. Therefore, it can be concluded  
335 that the numerical analysis is able to predict the shear buckling forces of the sections with good  
336 accuracy.

337 Further, Fig. 6 plots the shear buckling coefficients of each section considered. It is seen from  
338 Fig. 6 that LCB sections with return lips have shear buckling coefficients which are almost  
339 equal to that of LCB sections. The ratio between the back-calculated shear buckling coefficient  
340 of the sections with return lips and the shear buckling coefficient derived from Eq. (5) for LCBs  
341 further confirm this with a mean of 1.00 and a COV of 0.006. According to Fig. 6, LCB sections  
342 with triangular and trapezoidal web stiffeners exhibits higher shear buckling coefficients  
343 compared to LCB sections. The sections with trapezoidal web stiffeners feature the highest  
344 coefficients among the considered sections. The variation of the magnitude of the shear  
345 buckling coefficients of web stiffened sections is associated with the variation of the web  
346 stiffener indent. Therefore, it can be concluded that the web stiffeners enhance the shear  
347 buckling resistance of the sections. Further, it is seen that the higher the indent of the web  
348 stiffener is, the higher the shear buckling coefficient.

349 Table 6 Elastic shear buckling analysis results

No.	Section	LCB			LCB-RL			LCB-TR			LCB-TP		
		$V_{cr,FE}$ (kN)	$k_{v,FE}$	$k_{v,FE}/$ $k_{LCB,Eq,(5)}$	$V_{cr,FE}$ (kN)	$k_{v,FE}$	$k_{v,FE}/$ $k_{LCB,Eq,(5)}$	$V_{cr,FE}$ (kN)	$k_{v,FE}$	$k_{v,FE}/$ $k_{LCB,Eq,(5)}$	$V_{cr,FE}$ (kN)	$k_{v,FE}$	$k_{v,FE}/$ $k_{LCB,Eq,(5)}$
1	Section 150×65×15×1.0	12.61	10.047	1.00	12.72	10.133	1.00	23.51	18.731	1.86	32.53	25.912	2.57
2	Section 150×65×15×1.2	21.80	10.021	0.99	21.98	10.105	1.00	36.13	16.610	1.65	50.15	23.053	2.28
3	Section 150×65×15×1.5	42.57	9.979	0.99	42.92	10.061	1.00	61.42	14.396	1.43	83.35	19.536	1.94
4	Section 150×65×15×2.0	100.92	9.909	0.98	101.69	9.985	0.99	125.09	12.283	1.22	157.26	15.442	1.53
5	Section 200×75×20×1.0	9.35	10.035	0.99	9.44	10.131	1.00	16.16	17.347	1.72	21.96	23.571	2.34
6	Section 200×75×20×1.2	16.16	10.017	0.99	16.32	10.112	1.00	25.04	15.523	1.54	33.85	20.982	2.08
7	Section 200×75×20×1.5	31.57	9.988	0.99	31.87	10.082	1.00	43.25	13.682	1.36	56.57	17.895	1.77
8	Section 200×75×20×2.0	74.87	9.940	0.99	75.55	10.031	0.99	90.23	11.979	1.19	109.12	14.487	1.44
9	Section 250×75×20×1.0	7.37	9.946	0.99	7.45	10.053	1.00	12.05	16.268	1.61	16.15	21.801	2.16
10	Section 250×75×20×1.2	12.74	9.932	0.98	12.87	10.036	0.99	18.82	14.680	1.45	24.89	19.411	1.92
11	Section 250×75×20×1.5	24.88	9.908	0.98	25.13	10.009	0.99	32.92	13.112	1.30	41.82	16.658	1.65
12	Section 250×75×20×2.0	58.98	9.870	0.98	59.53	9.962	0.99	69.81	11.683	1.16	82.14	13.746	1.36
	Mean		9.966	0.99		10.058	1.00						
	COV		0.006	0.006		0.006	0.006						

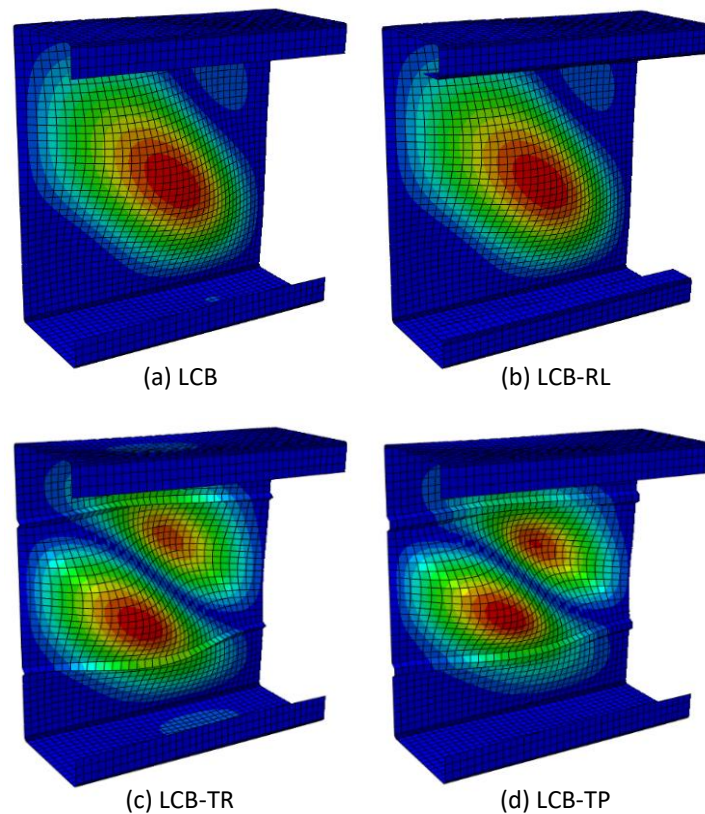


351

352 Fig. 6 Comparison of shear buckling coefficients of different sections

353 5.4 Shear buckling modes

354 Fig. 7 illustrates the identified critical elastic shear buckling modes of each section. From Figs.  
 355 7 (a) and (b), it can be seen that both plain LCBs and LCBs with return lips have similar shear  
 356 buckling modes with single buckling half-waves. Further, it can be observed that the shear  
 357 buckling modes of LCBs with triangular and trapezoidal web stiffeners are similar to each other  
 358 from Figs. 7 (c) and (d). However, LCB sections with longitudinal web stiffeners exhibit two  
 359 buckling half-waves. Therefore, it can be concluded that the presence of longitudinal web  
 360 stiffeners reduces the length of buckling half-waves of the section. However, the shape of the  
 361 stiffener does not have any significant effect on the buckling half-wave length of the section as  
 362 observed from Fig. 7. Moreover, the spreading of the buckling mode over the whole web and  
 363 the buckling of the web stiffeners can be observed in web stiffened LCB sections.



364

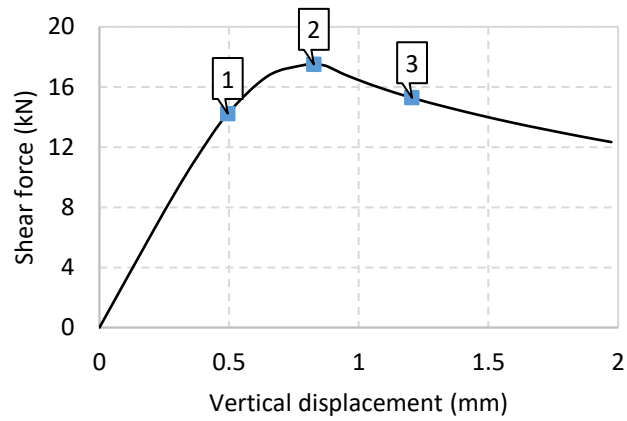
365 Fig. 7 Elastic shear buckling modes of different cross-sections

## 366 6 Analysis of FE shear failure modes

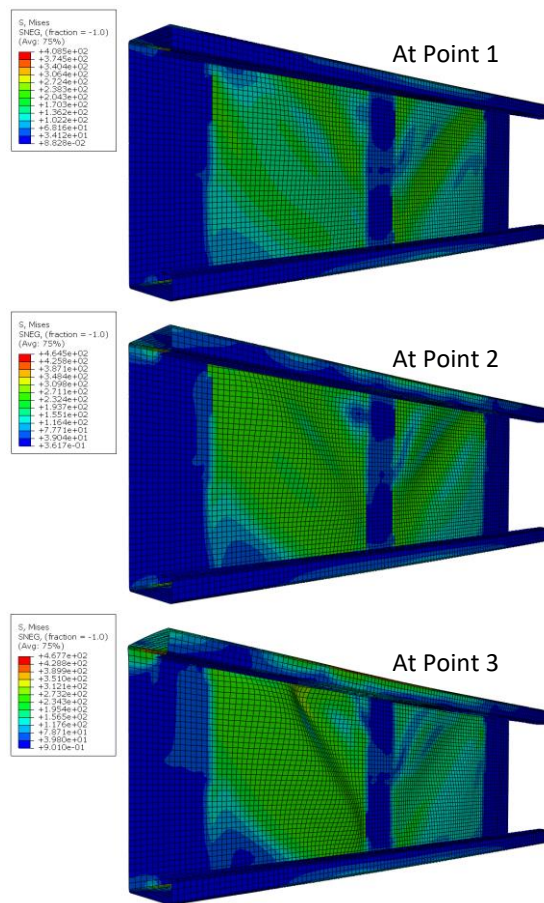
367 The structural behaviour of the cold-formed stainless steel stiffened channel sections subjected  
 368 to shear was investigated in this section using numerical results generated in the parametric  
 369 study. The failure mechanism of each different section type was observed at different stages of  
 370 the load-deflection curve. Figs. 8-10 illustrate the failure mechanisms of each section type  
 371 investigated in this study alongside their load-deflection curves. From Fig. 8, it can be observed  
 372 that the shear buckling of both webs of LCB-RL 200×75×20×1.0 section with return lips. The  
 373 out-of-plane buckling of webs was approximately started at Point 1 of the load-deflection curve  
 374 and the progression of the web buckling was observed when the section reaches the post-peak  
 375 loading region.

376 Figs. 9 and 10 depict the web shear buckling of channel sections with triangular and trapezoidal  
 377 web stiffeners. The buckling of the web stiffener above the neutral axis can be observed for  
 378 both sections with triangular and trapezoidal stiffeners as a result of compressive stresses in  
 379 the sections. This is because the stiffness of the web stiffeners is not large enough to resist the  
 380 out-of-plane buckling induced by the compressive stresses. A shift of the buckling pattern

381 towards the top half of the section webs can be seen with the presence of a web stiffener below  
 382 the neutral axis. The web stiffener below the neutral axis was able to minimise the out-of-plane  
 383 buckling of the webs at the post-buckling region with the aid of tensile stresses developed in  
 384 the section.



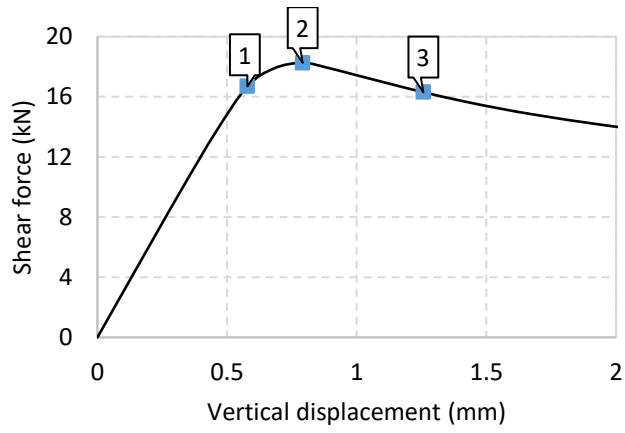
(a) Load-Deflection curve



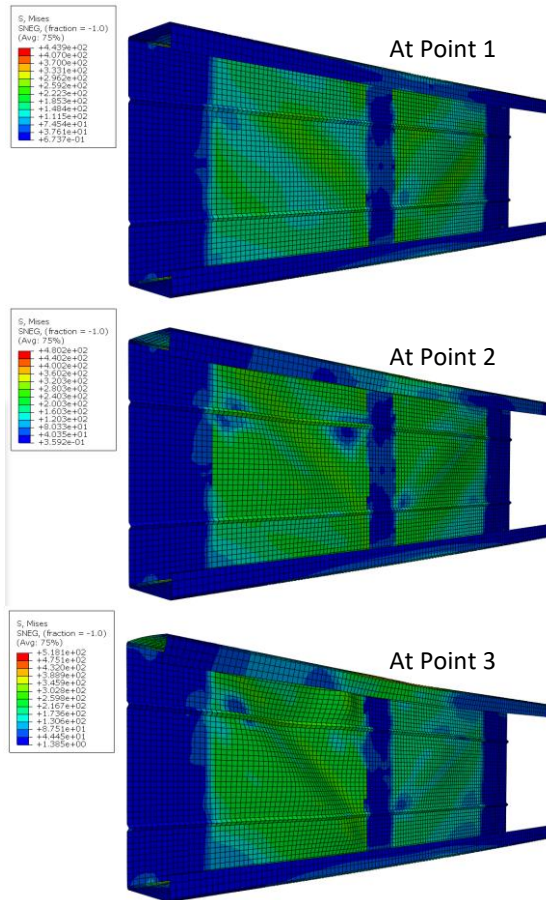
(b) FE shear failure modes

385

386 Fig. 8 FE shear failure modes of LCB-RL 200×75×20×1.0 section at the different stages of the load-deflection  
 387 curve



(a) Load-Deflection curve

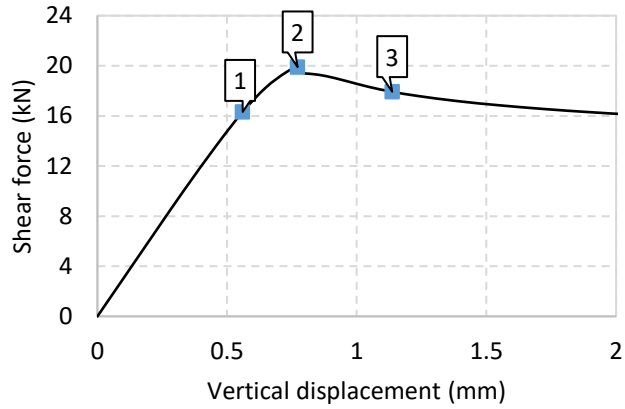


(b) FE shear failure modes

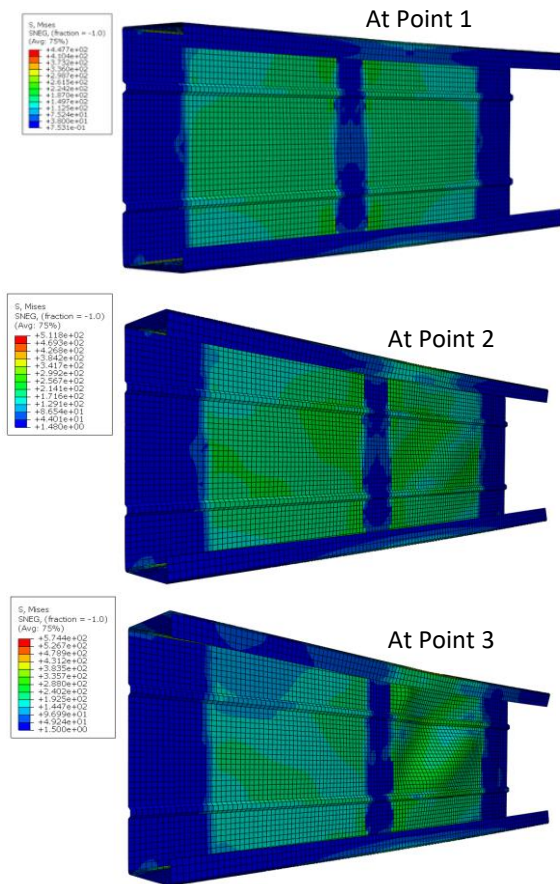
388

389 Fig. 9 FE shear failure modes of LCB-TR 200×75×20×1.0 section at the different stages of the load-deflection

390 curve



(a) Load-Deflection curve



(b) FE shear failure modes

391

392 Fig. 10 FE shear failure modes of LCB-TP 200×75×20×1.0 section at the different stages of the load-deflection  
 393 curve

## 394 7 Evaluation of shear design provisions

395 This section covers the evaluation of EN1993-1-4 [5] and the DSM shear design provisions for  
 396 cold-formed stainless steel channel sections with stiffeners investigated in the parametric study.

397 The generated numerical results were compared with the code predictions, and modifications



398 were applied to the codified rules where necessary to enhance the resistance prediction  
 399 accuracy.

#### 400 7.1 EN1993-1-4 shear design provisions

401 The shear design provisions provided in European standards for stainless steel, EN1993-1-4  
 402 [5] refer to the shear design equations set out in EN1993-1-5 [6] which are based on the rotated  
 403 stress field method. In EN1993-1-5 [6], the shear resistance ( $V_{b,Rd}$ ) of a section is defined as  
 404 the summation of the web shear buckling resistance ( $V_{bw,Rd}$ ) and the flange contribution to the  
 405 shear resistance ( $V_{bf,Rd}$ ). This is expressed in Eq. (6).

$$406 \quad V_{b,Rd} = V_{bw,Rd} + V_{bf,Rd} \leq \frac{\eta f_{yw} h_w t_w}{\sqrt{3} \gamma_{M1}} \quad (6)$$

407 where  $f_{yw}$  is the yield strength of the web,  $h_w$  is the web depth,  $t_w$  is the web thickness and  $\gamma_{M1}$   
 408 is the partial safety factor. The parameter ‘ $\eta$ ’ takes into account the strain hardening of stainless  
 409 steel.

410 The web shear buckling resistance,  $V_{bw,Rd}$  is defined by Eq. (7).

$$411 \quad V_{bw,Rd} = \frac{\chi_w f_{yw} h_w t_w}{\sqrt{3} \gamma_{M1}} \quad (7)$$

412 where  $\chi_w$  is the web shear buckling reduction factor.

413 In EN1993-1-4 [5], separate expressions are provided for web shear buckling reduction factor,  
 414  $\chi_w$  as a function of the web slenderness,  $\bar{\lambda}_w$  and these expressions for web panels with rigid end  
 415 post are given by Eqs. (8)-(10).

$$416 \quad \chi_w = \eta \text{ for } \bar{\lambda}_w \leq 0.65/\eta \quad (8)$$

$$417 \quad \chi_w = 0.65/\bar{\lambda}_w \text{ for } 0.65/\eta < \bar{\lambda}_w < 0.65 \quad (9)$$

$$418 \quad \chi_w = 1.56/(0.91 + \bar{\lambda}_w) \text{ for } \bar{\lambda}_w \geq 0.65 \quad (10)$$

419 In EN1993-1-5 [6], Eq. (11) is used for the calculation of slenderness ( $\bar{\lambda}_w$ ) of the webs with  
 420 both transverse stiffeners and longitudinal stiffeners.

$$421 \quad \bar{\lambda}_w = \frac{h_w}{37.4 t_w \varepsilon \sqrt{k_\tau}} \quad (11)$$

422 where  $\varepsilon$  is the material factor and  $k_\tau$  is the web shear buckling coefficient.

423 The flange contribution to the section shear resistance,  $V_{bf,Rd}$  is given by Eq. (12) which is  
 424 applied only when the design bending moment ( $M_{Ed}$ ) of the section is less than the bending  
 425 resistance of the flanges alone ( $M_{f,Rd}$ ).

$$426 \quad V_{bf,Rd} = \frac{b_f t_f^2 f_{yf}}{c \gamma_{M1}} \left( 1 - \left( \frac{M_{Ed}}{M_{f,Rd}} \right)^2 \right) \quad (12)$$

427 where  $b_f$  is the flange width,  $t_f$  is the flange thickness and  $f_{yf}$  is the yield stress of the flange.

428 The distance along the flange from the transverse stiffener to the location of the plastic hinge  
 429 is expressed by the parameter 'c'. An alternative expression for 'c' is defined in EN1993-1-4  
 430 [5] and given in Eq. (13).

$$431 \quad c = a \left[ 0.17 + \frac{3.5 b_f t_f^2 f_{yf}}{t_w h_w^2 f_{yw}} \right] \text{ and } \frac{c}{a} \leq 0.65 \quad (13)$$

432 where a is the spacing between transverse stiffeners.

433 Then, numerical shear capacities for cold-formed LCB sections with stiffeners were compared  
 434 with EN1993-1-4 [5] predictions. For the calculation of EN1993-1-4 [5] shear capacities, the  
 435 back-calculated shear buckling coefficients found from the numerical shear buckling analysis  
 436 conducted in Section 5 were incorporated. Tables 3-5 summarise the ratio between the FE shear  
 437 capacity and EN1993-1-4 [5] predicted shear capacity of each section for each stainless steel  
 438 grade while Table 7 compares the overall mean and COV values for each section type. From  
 439 the comparison, it was found that the FE shear capacity to EN1993-1-4 [5] predicted shear  
 440 capacity ratio for LCBs with return lips have a mean and a COV of 1.10 and 0.024, respectively.  
 441 Further, the mean and the COV of the FE shear capacity to the predicted shear capacity ratio  
 442 for LCBs with triangular web stiffeners are 1.02 and 0.034, respectively while those values for  
 443 LCBs with trapezoidal web stiffeners are 0.97 and 0.047, respectively.

444

445

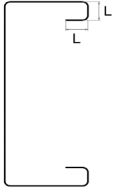
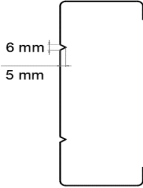
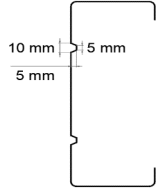
446

447

448

449

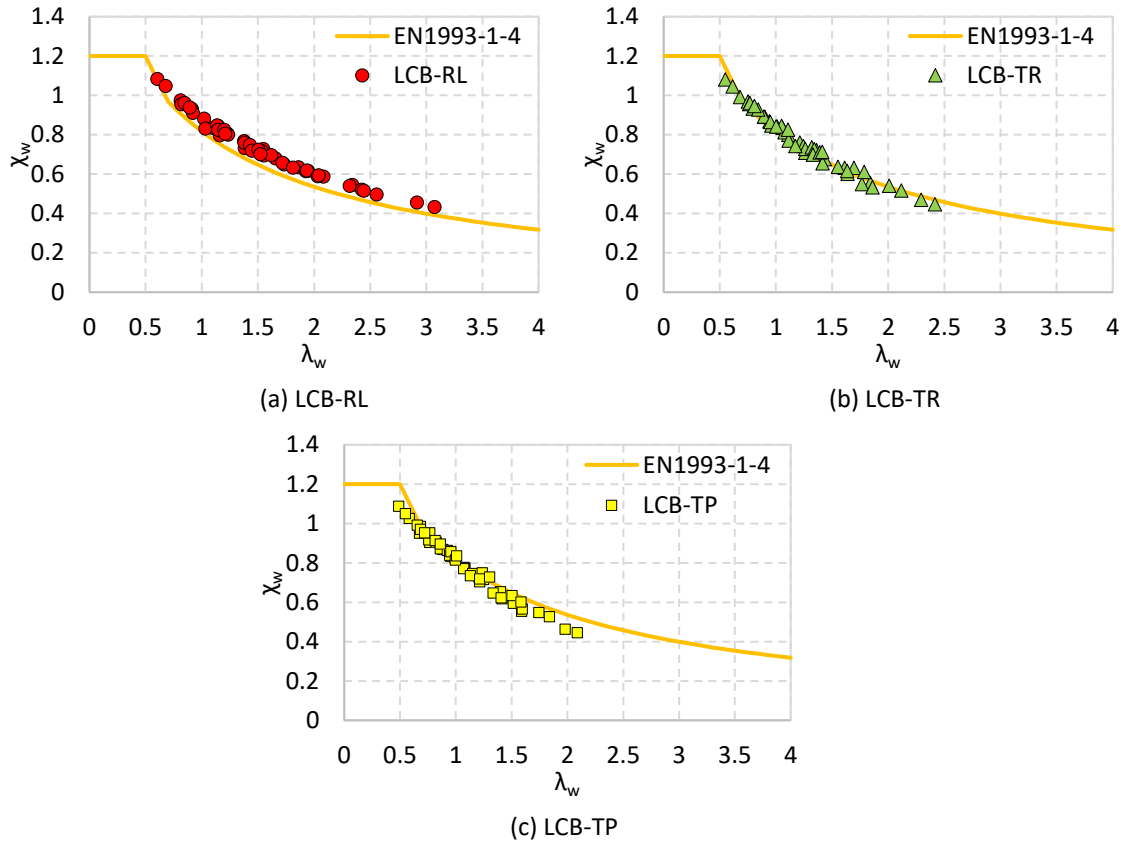
450 Table 7 Overall mean and COV values of FE to predicted resistance ratio for each section type

	LCB-RL		LCB-TR		LCB-TP	
	Current	Proposed	Current	Proposed	Current	Proposed
						
EN1993-1-4 [5]						
Mean	1.10	1.00	1.02	1.01	0.97	0.99
COV	0.024	0.014	0.034	0.022	0.047	0.035
DSM						
Mean	1.07	1.00	0.98	1.02	0.93	0.98
COV	0.045	0.025	0.034	0.031	0.040	0.043

451

452 Fig. 11 compares the FE shear capacities with EN1993-1-4 [5] web shear buckling reduction  
 453 factor ( $\chi_w$ ) curve for all three section types. The comparison of FE shear capacities with the  
 454 code predictions suggests that EN1993-1-4 [5] shear provisions are conservative for the cold-  
 455 formed stainless steel LCB sections with return lips. Further, EN1993-1-4 [5] shear design  
 456 rules are found to be satisfactory for the LCB sections with triangular web stiffeners, however,  
 457 it is concluded from the comparisons that the shear capacities of LCB sections with trapezoidal  
 458 web stiffeners are over-predicted.

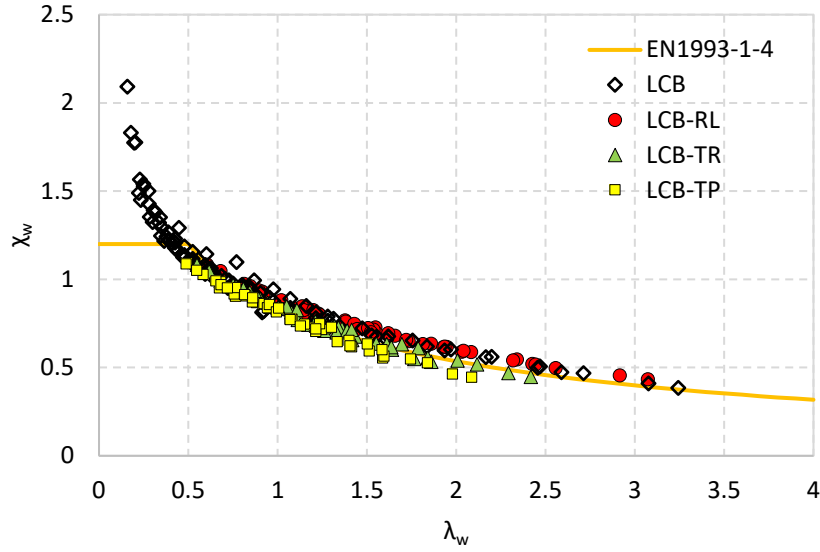
459



460

461 Fig. 11 Comparison of FE shear capacities with EN1993-1-4 [5] curve for web shear buckling reduction factor,  
 462  $\chi_w$

463 Dissanayake et al. [13] conducted numerical studies on the shear behaviour of cold-formed  
 464 stainless steel LCB sections and proposed new design equations. In Fig. 12, the FE results of  
 465 shear capacities generated for all three section types are compared with the experimental and  
 466 FE shear capacities of cold-formed stainless steel LCB sections found from Dissanayake et al.  
 467 [13]. It can be seen that there is no significant enhancement in the shear resistance of cold-  
 468 formed stainless steel LCB sections with stiffeners considered in this study compared to plain  
 469 LCB sections. In addition, FE data points shifted along the x-axis with the reduced web  
 470 slenderness ( $\bar{\lambda}_w$ ) as a result of the higher shear buckling coefficient ( $k_v$ ) of the sections with  
 471 web stiffeners.



472

473 Fig. 12 Comparison of FE shear capacities of stainless steel stiffened LCBs with the experimental and FE shear  
 474 capacities of plain LCBs found from Dissanayake et al. [13]

475 Following the evaluation of EN1993-1-4 [5] shear design provisions in predicting the shear  
 476 resistance of cold-formed stainless steel LCB sections with longitudinal stiffeners,  
 477 modifications were proposed to EN1993-1-4 [5] web shear buckling reduction factor ( $\chi_w$ ) to  
 478 enhance the prediction accuracy. For this, web shear buckling resistance ( $V_{bw,Rd}$ ) defined by  
 479 Eq. (7) was directly compared with the FE shear capacities as the flange contribution ( $V_{bf,Rd}$ )  
 480 to the shear resistance of the section given by Eq. (12) was negligible. Two separate sets of  
 481 expressions were proposed for the web shear buckling reduction factor ( $\chi_w$ ) after following  
 482 regression analyses. The slenderness limits were defined accordingly in each case at the yield  
 483 load of the sections.

484 The proposed expressions for LCB sections with return lips are given by Eqs. (14)-(16).

$$485 \quad \chi_w = \eta \text{ for } \bar{\lambda}_w \leq 0.65/\eta \quad (14)$$

$$486 \quad \chi_w = 0.874/\bar{\lambda}_w^{0.517} \text{ for } 0.65/\eta < \bar{\lambda}_w < 0.77 \quad (15)$$

$$487 \quad \chi_w = 1.84/(1.07 + \bar{\lambda}_w) \text{ for } \bar{\lambda}_w \geq 0.77 \quad (16)$$

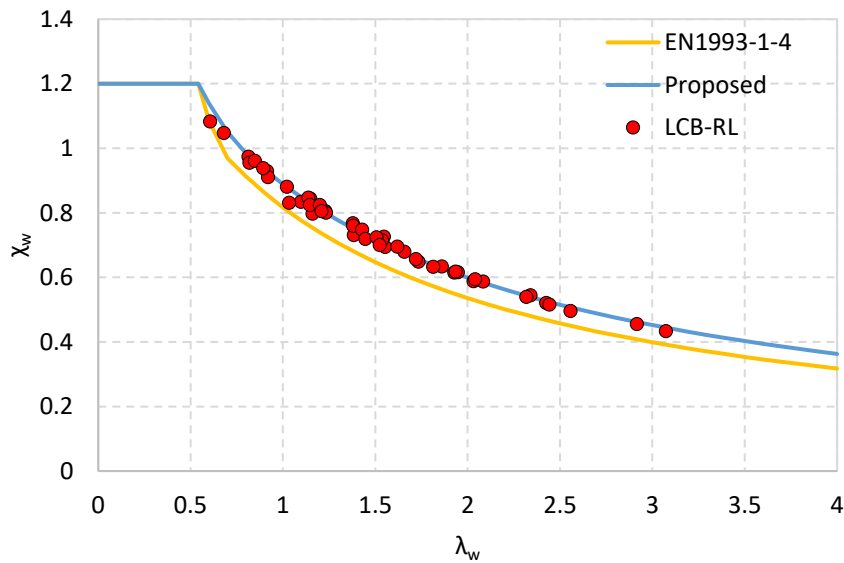
488 Then, another set of equations was proposed for LCB section with web stiffeners and is given  
 489 by Eqs. (17)-(19). In addition to web slenderness ( $\bar{\lambda}_w$ ), these proposed expressions depend on  
 490 the shear buckling coefficients ( $k_v$ ) of the sections as well.

$$491 \quad \chi_w = \eta \text{ for } \bar{\lambda}_w \leq 0.4 \quad (17)$$

492  $\chi_w = 0.868/\bar{\lambda}_w^{0.353}$  for  $0.4 < \bar{\lambda}_w < 0.67$  (18)

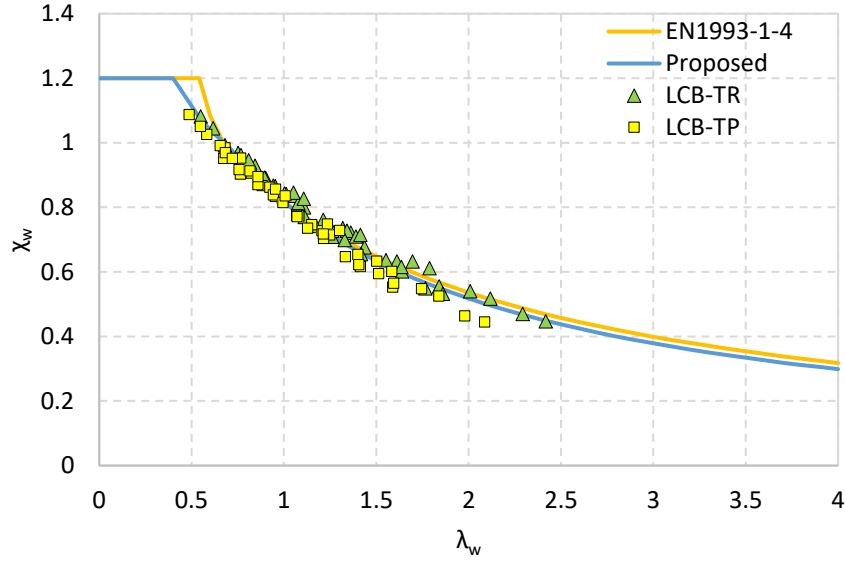
493  $\chi_w = 1.52/[(0.73 + \bar{\lambda}_w)(k_v/10.09)^{0.14}]$  for  $\bar{\lambda}_w \geq 0.67$  (19)

494 Figs. 13 and 14 compare the proposed curves for web shear buckling reduction factor with the  
 495 FE shear capacities of corresponding LCB sections. The average curve is plotted in Fig. 14  
 496 since Eq. (19) is a function of the shear buckling coefficient of each section. It can be seen that  
 497 proposed curves agree well with the distribution of the FE data points. The FE shear capacity  
 498 to the predicted shear capacity ratio of each section of each steel grade is listed for each set of  
 499 proposed expressions in Tables 3-5. From the calculation, it was found that the mean and the  
 500 COV of the FE shear capacity to the predicted shear capacity ratio are 1.00 and 0.014,  
 501 respectively for Eqs. (14)-(16) while the FE shear capacity to the predicted shear capacity ratio  
 502 has a mean and a COV of 1.00 and 0.028, respectively for Eqs. (17)-(19). Therefore, it can be  
 503 concluded that proposed expressions for EN1993-1-4 [5] web shear buckling reduction factor  
 504 ( $\chi_w$ ) are able to accurately predict the shear resistance of the considered LCB sections with  
 505 stiffeners and provide increased accuracy over the codified expressions.



506

507 Fig. 13 Comparison of FE shear capacities of LCB-RL sections with the proposed curve for EN1993-1-4 [5] web  
 508 shear buckling reduction factor,  $\chi_w$



509

510 Fig. 14 Comparison of FE shear capacities of LCB-TR and LCB-TP sections with the proposed curve for EN1993-  
 511 1-4 [5] web shear buckling reduction factor,  $\chi_w$

512 7.2 The DSM shear design provisions

513 In the DSM, all the elastic instabilities of the gross cross-section are taken into account to  
 514 determine the section strength. The DSM shear design provisions for the sections with  
 515 transverse web stiffeners are provided in the clause 7.2.3.3 of AS/NZS 4600 [11]. Eqs. (20)  
 516 and (21) defines the shear strength ( $V_v$ ) of a section according to the DSM.

517 
$$V_v = V_y \text{ for } \lambda \leq 0.776 \tag{20}$$

518 
$$V_v = \left[ 1 - 0.15 \left( \frac{1}{\lambda^2} \right)^{0.4} \right] \left( \frac{1}{\lambda^2} \right)^{0.4} V_y \text{ for } \lambda > 0.776 \tag{21}$$

519 where  $\lambda$  is the slenderness of the cross-section.

520 The slenderness ( $\lambda$ ) of the section can be calculated from Eq. (22) by determining the yield  
 521 strength ( $V_y$ ) and the elastic shear buckling strength ( $V_{cr}$ ) of the section.

522 
$$\lambda = \sqrt{\frac{V_y}{V_{cr}}} \tag{22}$$

523 The yield strength ( $V_y$ ) of the section is given by Eq. (23).

524 
$$V_y = 0.6 f_{yw} d_1 t_w \tag{23}$$

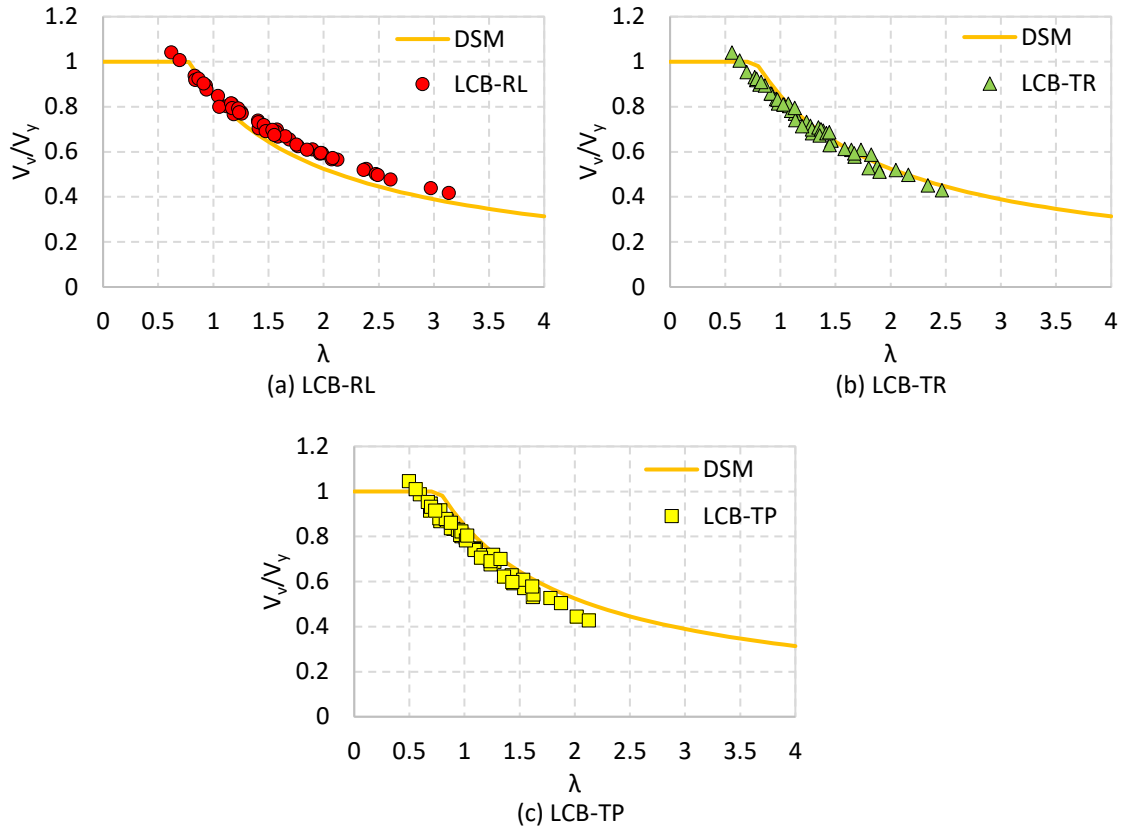
525 where  $d_1$  is the flat depth of the web.

526 For the calculation of the elastic shear buckling strength ( $V_{cr}$ ), Eq. (4) given in Section 5.3 can  
527 be used. Further, numerical analysis can also be conducted to find out the elastic shear buckling  
528 strength as described previously in Section 5.

529 Then, the DSM shear design provisions were compared with the FE shear capacities of cold-  
530 formed stainless steel LCB sections with stiffeners in this section. For the calculation of DSM  
531 shear capacities, back-calculated shear buckling coefficients were utilised from Section 5. The  
532 ratio between the FE shear capacity and the predicted shear capacity from the DSM of each  
533 section for each steel grade studied is given in Tables 3-5. The overall mean and COV values  
534 for each section type are compared in Table 7. The mean and the COV of the FE shear capacity  
535 to the DSM shear capacity ratio of LCB sections with return lips are found to be 1.07 and 0.045,  
536 respectively. Further, the FE shear capacity to the DSM shear capacity ratio for LCBs with  
537 triangular stiffeners has a mean and a COV of 0.98 and 0.034, respectively while that of LCBs  
538 with trapezoidal stiffeners are 0.93 and 0.040, respectively.

539 Fig. 15 illustrates the FE shear capacities of each LCB section type analysed with the DSM  
540 shear design curve. It can be concluded from all these comparisons of FE shear capacities with  
541 the DSM predictions that the DSM shear design rules are conservative for cold-formed stainless  
542 steel LCB sections with return lips while the DSM shear design provisions over-predict the  
543 shear capacities of LCB sections with longitudinal web stiffeners studied.





544

545 Fig. 15 Comparison of FE shear capacities with the DSM shear design curve

546 The modified DSM equations were also proposed to enhance the shear capacity prediction  
 547 accuracy of the cold-formed stainless steel LCB sections with stiffeners using FE results. After  
 548 conducting regression analyses to fit the distribution of FE data points, two sets of equations  
 549 were proposed by modifying Eqs. (20) and (21).

550 Eqs. (24) and (25) give the proposed DSM equations for LCB sections with return lips.

551 
$$V_v = V_y \text{ for } \lambda \leq 0.776 \tag{24}$$

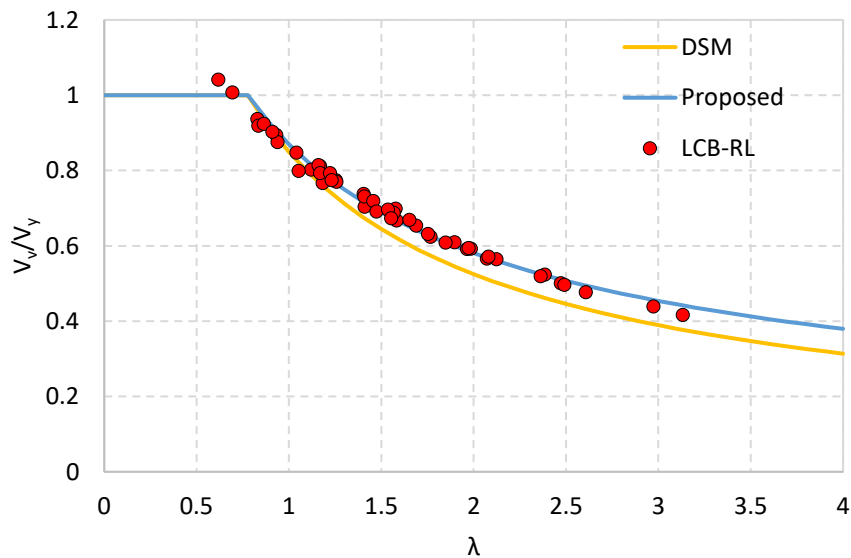
552 
$$V_v = \left[ 1 - 0.13 \left( \frac{1}{\lambda^2} \right)^{0.33} \right] \left( \frac{1}{\lambda^2} \right)^{0.33} V_y \text{ for } \lambda > 0.776 \tag{25}$$

553 Considering the FE results of LCB sections with web stiffeners, Eqs. (26) and (27) were  
 554 proposed to predict their shear capacities. Similar to the proposed EN1993-1-4 [5] expression  
 555 for the web shear buckling reduction factor of web stiffened LCB sections given by Eq. (19),  
 556 the proposed DSM equation expressed in Eq. (27) is also a function of both slenderness ( $\lambda$ ) and  
 557 shear buckling coefficient ( $k_v$ ) of the section.

558 
$$V_v = V_y \text{ for } \lambda \leq 0.66 \tag{26}$$

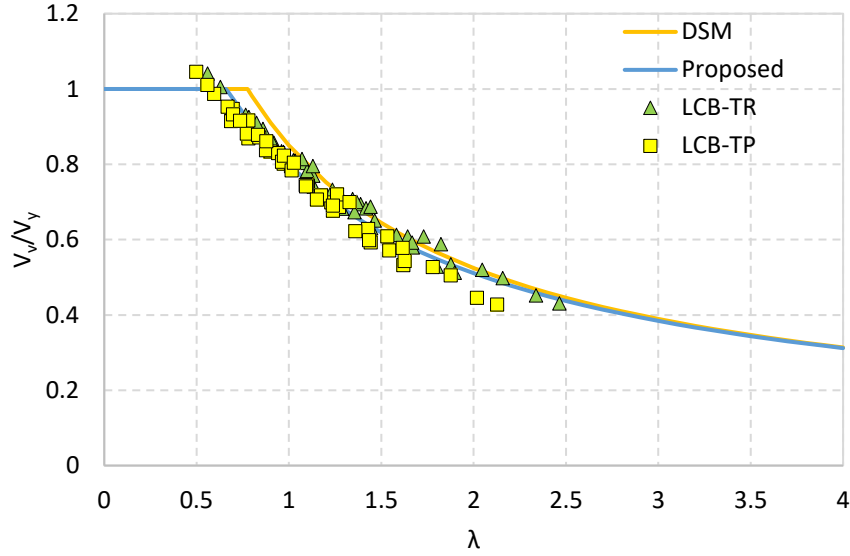
559 
$$V_v = \left[ 1 - 0.16 \left( \frac{k_v}{10.09} \right)^{0.45} \left( \frac{1}{\lambda^2} \right)^{0.395} \right] \left( \frac{1}{\lambda^2} \right)^{0.395} V_y \text{ for } \lambda > 0.66 \quad (27)$$

560 The proposed DSM equations were compared with the FE shear capacities of the respective  
 561 sections in Figs. 16 and 17. The average curve for Eq. (27) is plotted in Fig. 17, because Eq.  
 562 (27) includes the shear buckling coefficient of the section. The comparison of the proposed  
 563 DSM curves agrees well with the distribution of the FE data points. Further, the FE shear  
 564 capacity to the predicted shear capacity ratios are given in Tables 3-5 for the proposed DSM  
 565 equations. It was calculated that the mean and the COV of the FE shear capacity to the predicted  
 566 shear capacity ratio are 1.00 and 0.025, respectively for Eqs. (24) and (25) while that of Eqs.  
 567 (26) and (27) are 1.00 and 0.034, respectively. Therefore, the proposed DSM equations provide  
 568 better shear capacity predictions with increased accuracy compared to the DSM shear design  
 569 equations given in Eqs. (20) and (21).



570

571 Fig. 16 Comparison of FE shear capacities of LCB-RL sections with the proposed DSM curve



572

573 Fig. 17 Comparison of FE shear capacities of LCB-TR and LCB-TP sections with the proposed DSM curve

574 7.3 Reliability analysis

575 The capacity reduction factors were calculated for the proposed resistance models according  
 576 to AISI S100 [12]. The method takes into account the effects of the uncertainties of the  
 577 proposed resistance models, numerical models, geometric and material properties when  
 578 determining the reduction factors. Eq. (28) is used to calculate the capacity reduction factor  
 579 ( $\phi_v$ ) in this method.

$$580 \quad \phi_v = 1.52M_m F_m P_m e^{-\beta_0 \sqrt{(V_m^2 + V_f^2 + C_p V_p^2 + V_q^2)}} \quad (28)$$

581 where

582  $M_m=1.1$  is the mean of the material factor

583  $V_m=0.1$  is the variation coefficient of the material factor

584  $F_m=1.0$  is the mean of the fabrication factor

585  $V_f=0.05$  is the variation coefficient of the fabrication factor

586  $P_m$  is the mean of the actual to predicted resistance ratio

587  $V_p$  is the variation coefficient of the actual to predicted resistance ratio (not less than 0.065)

588  $\beta_0$  is the target reliability index

589  $V_q=0.21$  is the variation coefficient of the load effect

590  $C_p$  is the correction factor and is given by Eq. (29).

$$591 \quad C_p = \left[ 1 + \frac{1}{n} \right] \left[ \frac{m}{m-2} \right] \quad (29)$$

592 where 'n' is the number of data points and  $m=n-1$  is the number of degrees of freedom.

593 The capacity reduction factors for the proposed EN1993-1-4 [5] and the DSM resistance  
594 models were calculated and are given in Table 8. The target reliability index,  $\beta_0$  was taken as  
595 2.5 for all the cases. The minimum recommended value was used for the variation coefficient,  
596  $V_p$  since the calculated values are less than 0.065 for all the resistance models. From the results,  
597 a capacity reduction factor of 0.90 can be recommended for all the proposed resistance models.

598 Table 8 Reliability analysis results

	Proposed EN1993-1-4 [5] resistance models		Proposed DSM resistance models	
	Eqs. (14)-(16)	Eqs. (17)-(19)	Eqs. (24) & (25)	Eqs. (26) & (27)
Capacity reduction factor ( $\phi_v$ )	0.901	0.902	0.901	0.902

## 599 8 Concluding remarks

600 The use of numerical modelling to investigate the shear response of cold-formed stainless steel  
601 LCB sections with longitudinal stiffeners was discussed. First, the developed FE models were  
602 validated with the shear tests of cold-formed stainless steel LCB sections found in the literature.  
603 Then, the elaborated FE models were utilised to study the shear behaviour of stiffened LCB  
604 sections in the numerical parametric study. The effect of return lips, and triangular and  
605 trapezoidal web stiffeners on the shear behaviour of LCB sections were comprehensively  
606 investigated for different stainless steel grades by generating a database of 144 FE models.  
607 Additionally, elastic shear buckling analyses were conducted for considered varying cross-  
608 sections using numerical modelling and shear buckling coefficients were back-calculated from  
609 the FE results.

610 From the observations of the shear buckling analysis, it was found that the back-calculated  
611 shear buckling coefficients ( $k_v$ ) of LCB sections with return lips are almost equal to that of  
612 plain LCB sections. The back-calculated coefficients for LCB sections with web stiffeners are  
613 significantly higher compared to plain LCB sections where the sections with trapezoidal web  
614 stiffeners feature the highest coefficients among considered sections. Furthermore, it was  
615 concluded that the higher the indent of the web stiffener is, the higher the shear buckling

616 coefficient. The observed shear buckling modes of LCB sections with return lips are found to  
617 be similar to that of plain LCB sections with single buckling half-waves while sections with  
618 web stiffeners have two buckling half-waves reducing the length of buckling half-waves. The  
619 spreading of the buckling half-waves over the whole web region was further observed, even  
620 with the presence of the web stiffeners.

621 It can be seen from the analysis of the shear failure modes of stiffened LCB sections that the  
622 buckling of web stiffeners located above the neutral axis of the section. Therefore, it was  
623 concluded that the stiffness of the longitudinal web stiffeners is not large enough to resist the  
624 out-of-plane buckling caused by the compressive stresses in the sections. Furthermore, it was  
625 observed that the shear capacity increment of the LCB sections with stiffeners is not significant  
626 compared to the plain LCB sections.

627 The evaluation of EN1993-1-4 [5] and the DSM shear design provisions suggested that the  
628 codified rules are conservative for cold-formed stainless steel LCB sections with return lips.  
629 Further, it was found that EN1993-1-4 [5] provisions over predict the shear capacities of LCB  
630 sections with trapezoidal web stiffeners while the DSM provisions over predict the shear  
631 capacities of LCB sections with both triangular and trapezoidal web stiffeners. Therefore, new  
632 provisions were proposed for EN1993-1-4 [5] web shear buckling reduction factor ( $\chi_w$ ) and the  
633 DSM shear design rules considering the FE results. The proposed design provisions provide  
634 enhanced shear resistance predictions with higher accuracy compared to the codified  
635 provisions.

## 636 **Acknowledgements**

637 Authors would like to thank Northumbria University for financial support and providing the  
638 necessary research facilities to conduct this research.

## 639 **References**

- 640 [1] C. H. Pham, L. A. Bruneau, G. J. Hancock, Experimental study of longitudinally  
641 stiffened web channels subjected to Combined Bending and Shear, *J. Struct. Eng.* 141  
642 (11) (2015).
- 643 [2] C. H. Pham, G. J. Hancock, Direct strength design of cold-formed C-sections for shear  
644 and combined actions, *J. Struct. Eng.* 138 (6) (2012) pp. 759–768.
- 645 [3] L. Wang, B. Young, Design of cold-formed steel channels with stiffened webs  
646 subjected to bending, *Thin-Walled Struct.* 85 (2014) pp. 81–92.

- 647 [4] S. H. Pham, C. H. Pham, G. J. Hancock, Direct strength method of design for shear  
648 including sections with longitudinal web stiffeners, *Thin-Walled Struct.* 81 (2014) pp.  
649 19–28.
- 650 [5] EN 1993-1-4:2006+A1:2015, Eurocode 3 – Design of steel structures – Part 1–4:  
651 General rules – Supplementary rules for stainless steels, European Committee for  
652 Standardization (CEN), Brussels, 2015.
- 653 [6] EN 1993-1-5, Eurocode 3 – Design of steel structures – Part 1–5: Plated structural  
654 elements, European Committee for Standardization (CEN), Brussels, 2006.
- 655 [7] T. Höglund, Behaviour and strength of the web of thin plate I-girders, Bulletin No. 93  
656 of the Division of Building Statics and Structural Engineering, The Royal Institute of  
657 Technology, Stockholm, Sweden, 1971, pp. 13–30.
- 658 [8] O. Zhao, S. Afshan, L. Gardner, Structural response and continuous strength method  
659 design of slender stainless steel cross-sections, *Eng. Struct.* 140 (2017) pp. 14–25.
- 660 [9] B. W. Schafer, S. Ádány, Buckling analysis of cold-formed steel members using  
661 CUFSM: conventional and constrained finite strip methods, Proceedings of the  
662 eighteenth international speciality conference on cold-formed steel structures, Orlando,  
663 USA, 2006.
- 664 [10] V. V. Nguyen, G. J. Hancock, C. H. Pham, Development of the Thin-Wall-2 program  
665 for buckling analysis of thin-walled sections under generalised loading, Proceedings of  
666 the eighth international conference on advances in steel structures, Lisbon, Portugal,  
667 2015.
- 668 [11] AS/NZS 4600, Cold-formed steel structures, Standards Australia/Standards New  
669 Zealand (AS/NZS), Sydney, 2018.
- 670 [12] AISI S100–16, North American Specification for the design of cold-formed steel  
671 structural members, American Iron and Steel Institute (AISI), Washington, 2016.
- 672 [13] D. M. M. P. Dissanayake, K. Poologanathan, S. Gunalan, K. D. Tsavdaridis, B.  
673 Nagaratnam, K. S. Wanniarachchi, Numerical modelling and shear design rules of  
674 stainless steel lipped channel sections, *J. Constr. Steel Res.* (2019) (In press).
- 675 [14] P. Keerthan, M. Mahendran, Experimental investigation and design of lipped channel  
676 beams in shear, *Thin-Walled Struct.* 86 (2015) pp. 174–184.
- 677 [15] P. Keerthan, M. Mahendran, Experimental studies on the shear behaviour and strength  
678 of LiteSteel beams, *Eng. Struct.* 32 (10) (2010) pp. 3235–3247.
- 679 [16] P. Keerthan, M. Mahendran, Shear behaviour and strength of LiteSteel beams with web  
680 openings, *Adv. Struct. Eng.* 15 (2) (2012) pp. 171–184.

- 681 [17] M. Mahendran, P. Keerthan, Experimental studies of the shear behavior and strength  
682 of LiteSteel beams with stiffened web openings, *Eng. Struct.* 49 (2013) pp. 840–854.
- 683 [18] ABAQUS 6.14 Analysis User’s Guide, Dassault Systèmes, Rhode Island, USA, 2014.
- 684 [19] C. H. Pham, G. J. Hancock, Numerical simulation of high strength cold-formed purlins  
685 in combined bending and shear, *J. Constr. Steel Res.* 66 (10) (2010) pp. 1205–1217.
- 686 [20] P. Keerthan, M. Mahendran, Numerical modeling of LiteSteel beams subject to shear,  
687 *J. Struct. Eng.* 137 (12) (2011) pp. 1428–1439.
- 688 [21] P. Keerthan, M. Mahendran, D. Hughes, Numerical studies and design of hollow flange  
689 channel beams subject to combined bending and shear actions, *Eng. Struct.* 75 (2014)  
690 pp. 197–212.
- 691 [22] C. H. Pham, G. J. Hancock, Numerical investigation of longitudinally stiffened web  
692 channels predominantly in shear, *Thin-Walled Struct.* 86 (2015) pp. 47–55.
- 693 [23] J. K. Sonu, K. D. Singh, Shear characteristics of Lean Duplex Stainless Steel (LDSS)  
694 rectangular hollow beams, *Structures* 10 (2016) pp. 13–29.
- 695 [24] I. Arrayago, E. Real, L. Gardner, Description of stress-strain curves for stainless steel  
696 alloys, *Mater. Des.* 87 (2015) pp. 540–552.
- 697 [25] R. B. Cruise, L. Gardner, Strength enhancements induced during cold forming of  
698 stainless steel sections, *J. Constr. Steel Res.* 64 (11) (2008) pp. 1310–1316.
- 699 [26] M. Ashraf, L. Gardner, D. A. Nethercot, Strength enhancement of the corner regions of  
700 stainless steel cross-sections, *J. Constr. Steel Res.* 61 (1) (2005) pp. 37–52.
- 701 [27] R. G. Dawson, A. C. Walker, Post-buckling of geometrically imperfect plates, *J. Struct.*  
702 *Div.* 98 (1) (1972) pp. 75–94.
- 703 [28] L. Gardner, D. A. Nethercot, Numerical modeling of stainless steel structural  
704 components—A consistent approach, *J. Struct. Eng.* 130 (10) (2004) pp. 1586–1601.
- 705 [29] EN 1993-1-3, Eurocode 3 – Design of steel structures – Part 1–3: General rules –  
706 Supplementary rules for cold-formed members and sheeting, European Committee for  
707 Standardization (CEN), Brussels, 2006.
- 708 [30] C. H. Pham, G. J. Hancock, Shear buckling of channels using the Semi-Analytical and  
709 Spline Finite Strip Methods, *J. Constr. Steel Res.* 90 (2013) pp. 42–48.
- 710 [31] G. J. Hancock, C. H. Pham, Shear buckling of channel sections with simply supported  
711 ends using the Semi-Analytical Finite Strip Method, *Thin-Walled Struct.* 71 (2013) pp.  
712 72–80.
- 713 [32] P. Keerthan, M. Mahendran, Shear buckling characteristics of cold-formed steel  
714 channel beams, *Int. J. Steel Struct.* 13 (3) (2013) pp. 385–399.

- 715 [33] P. Keerthan, M. Mahendran, Improved shear design rules of cold-formed steel beams,  
716 Eng. Struct. 99 (2015) pp. 603–615.
- 717 [34] S. Timoshenko, J. Gere, Theory of Elastic Stability, McGraw Hill, New York, USA,  
718 1961.